Molecular interactions, characterization and photoactivity of Chlorophyll *a*/Chitosan/2-HP-β-Cyclodextrin composite films as functional and active surfaces for ROS production.

Vito Rizzi[a], *Paola Fini*[b], *Fiorenza Fanelli*[c], *Tiziana Placido*[a], *Paola Semeraro*[a], *Teresa Sibillano*[d], *Aurore Fraix*[e], *Salvatore Sortino*[e], *Angela Agostiano*[a,b], *Cinzia Giannini*[d], *Pinalysa Cosma*[a,b]*.

[a]*Università degli Studi "Aldo Moro" di Bari, Dip. Chimica, Via Orabona, 4- 70126 Bari, Italy.*

[b]*Consiglio Nazionale delle Ricerche CNR-IPCF, UOS Bari, Via Orabona, 4- 70126 Bari, Italy.*

[c]*Consiglio Nazionale delle Ricerche CNR-NANOTEC, UOS Bari, Via Orabona, 4- 70126 Bari, Italy.*

[d]*Consiglio Nazionale delle Ricerche CNR-IC, Via Amendola 122/O- 70126 Bari, Italy*

[e]*Laboratory of Photochemistry, Department of Drug Sciences, University of Catania, Viale Andrea Doria 6, I-95125 Catania, Italy*

ABSTRACT

Novel photosensitizing film based on the natural hybrid polymer Chitosan/2-hydroxy-propyl-β-Cyclodextrin (CH/CD) is synthesized introducing Chlorophyll *a* (CH/CD/Chl*a*) as a photoactive agent for possible application in antimicrobial photodynamic therapy (PDT). The polymer

absorbs visible light, in turn able to generate reactive oxygen species (ROS) and, therefore it can be used as environmental friendly and biodegradable polymeric photosensitizer (PS). The modified film is characterized by means of different spectroscopic, calorimetric, diffraction techniques and microscopic imaging methods including time-resolved absorption spectroscopy. UV-Vis, FTIR-ATR and X-ray Photoelectron Spectroscopy (XPS) analyses suggest that Chl*a* shows a strong affinity toward Chitosan introducing interactions with amino groups present on the polymer chains. Nanosecond laser flash photolysis technique provides evidence for the population of the excited triplet state of Chl*a*. Photogeneration of singlet oxygen is demonstrated by both direct detection by using infrared luminescence spectroscopy and chemical methods based on the use of suitable traps. Scanning Electron Microscopy (SEM), Atomic Force Microscopy (AFM) and Differential Scanning Calorimetry (DSC) analyses confirm also the occurrence of structural changes both on the film surface and within the film layer induced by the insertion of the pigment. Moreover, X-ray Diffraction data (XRD) shows the existence of an amorphous phase for the chitosan films in all the compared conditions.

Keywords: Chitosan films, Chlorophyll a, active packaging, Singlet Oxygen, Cyclodextrins.

1. Introduction

Since several years, the problem involving the emergence of antibiotic resistance among pathogenic bacteria (Yoshikawa, 2002; Hamblin & Hasan, 2004), seems to lead to the end. Indeed, in several institutions around the world a more effective alternative for antibacterial treatments have been developed (Cerveny, De Paola, Duckworth & Gulig, 2002; Sajjan et al., 2001; Wainwright, 1998). Among them, Photodynamic Therapy (PDT), *i.e.* the combination of a

light source with a photosensitizing agent (PS) and endogenous molecular oxygen is considered as a practical therapy for these diseases (Rizzi et al. 2014; Fu, Jordan & Samson, 2013). In fact, the rapid growth and mutations of bacteria, able to facilitate microbes surviving in the presence of an antibiotic drug, will quickly become predominant throughout the microbial population. Additionally, since the indiscriminate and inappropriate use of antibiotics, the problem get worse (Yoshikawa, 2002). Interestingly, for recent years PDT has appeared useful for treatments of several problems as for example those related to food safety, in which a significant number of man-made activities could induce the contamination of food products (Balali, Grelier, Benaissa & Coma, 2008). As a consequence, the concept of Active Packaging becomes an interesting alternative to the traditional use of the conventional package, *i.e.* a passive barrier protecting the food. In European Community such new innovative concept has been defined as ‘‘a type of packaging that changes the condition of the packaging to extend shelf-life or improve safety or sensory properties while maintaining the quality of the food’’ (Vermeiren, Devlieghere, Van Beest, de Kruijf & Debevere, 1999; Gomez-Estaca, Lopez-de-Dicastillo, Hernandez-Munoz, Catala & Gavara, 2014). In general, active food packaging provides additional functions that do not exist in conventional packaging systems and not only protect food passively and physically against environmental agents, but also inhibits or retards bacteria growth. Among different active packaging approaches (Vermeiren et al., 1999; Gomez-Estaca et al., 2014), the incorporation of active substances to the packaging material is an attractive development. Not surprisingly, the quality of packaged foods can be improved by controlling the release of these active agents reducing the growth rate of dangerous micro-organisms or inactivating it by contact (Quintavalla & Vicini, 2002). On the other hand, due to the decrease of fossil resources, the food packaging materials based on natural macromolecules from renewable resources have received great

attention (Coma, 2013; Pedersen, Stæhr Wernberg, &Thomsen, 2005). In fact, in recent years and in different fields, the main attention has been focused on the Biomass, occurring to be a renewable energy source (Coma, 2013; Pedersen et al., 2005). In such context, the attention of this paper has been focused on Chitosan (CH) as inexpensive, biodegradable, biocompatible, nontoxic and environmentally friendly linear amino polysaccharide derived from chitin, a major component of insects and crustacean shells. CH was chosen among biopolymers for the high-quality film forming properties and antimicrobial activity (Bordenave, Grelier, Pichavant & Coma, 2005; Bordenave, Grelier & Coma, 2010) useful for several applications (Moczek & Nowakowska, 2007; Rabea, Badawy, Stevens, Smagghe & Steurbaut, 2003). CH contains more than 5000 glucosamine units and it is obtained commercially from shrimp and crab shell chitin (a N-acetylglucosamine polymer) by alkaline deacetylation. For several years, bioactive CH matrices have been used in food preservation (Rabea et al., 2003; El Ghaouth, Arul, Grenier & Asselin, 1992; Muzzarelli & Rocchetti, 1986; Davies, Elson & Hayes, 1989; El Ghaouth, Arul, Ponnampalam & Boulet, 1991; Jiang & Li, 2001). More specifically, in recent years, the CH chemical modification by inserting photoactive groups acting as potential PS for application in photosensitized oxidation reactions in water has been developed (Moczek & Nowakowska, 2007).

The pioneering works of Krausz *and co-workers* (Mbakidi & Sol, 2013), and related references, highlight the interest in this field of research, also in the recent past. For example, Krouit *and co-workers* (Krouit & Krausz,2006) showed their new photoantimicrobial films composed of porphyrinated lipophilic cellulose esters and also the photobactericidal films from porphyrins grafted to alkylated cellulose (Krouit & Krausz, 2009).

89 Many kind of applications can be listed, however among them it is worth mentioning the work of
90 Ringot *and co-workers* (Ringot & Krausz, 2011) highlighting that porphyrins maintain their
91 properties as PSs when grafted to polysaccharides, *i.e.* chitosan or cellulose, obtaining modified
92 polymers as photobactericidal membranes or films for various applications.

93 Starting from results obtained by Krausz, and thanks to our experience on a natural chlorine,
94 Chl*a*, solubilized in different systems, (Agostiano, Catucci, Cosma & Fini, 2003; Agostiano et
95 al.,2002a; Dentuto et al., 2007) the development of CH film containing such pigment, for
96 potential application as bioactive antimicrobial packaging material, is presented for the first time
97 in this paper as a novel photoactive system. Nonetheless the excellent CH properties, the system
98 Chl*a*/CH presents several limitations due to the acid pH condition necessary for the preparation
99 of CH hydrogel. In fact, CH is insoluble in water, but soluble in dilute organic acids which
100 induce the protonation of CH free amino groups (Rabea et al., 2003), with pH condition not
101 suitable for the chemical stability of Chl*a*. Hence the standard procedure used in literature to
102 prepare CH films from hydrogel was modified in order to optimize the condition for introducing
103 Chl*a*.

104 It is ascertained in literature that CH films (indicated in the text as CH STD) were generally
105 prepared by the method described by B. Krajewska (Krajewska, Leszko & Zaborska, 1990;
106 Krajewska, 1991) in which a 1% (v/v) solution of CH is dissolved in 0.8% (v/v) aqueous acetic
107 acid solution. The acidity of the medium is too high and induces the chemical degradation of
108 Chl*a* with the release of the central Mg atom, inducing the loss of the chemical properties of the
109 pigment. In our proposed procedure the pH of CH hydrogel is maintained at about 6 units, value
110 at which Chl*a* is chemically stable. 2-HP-β-CD (or CD) has been used to promote chitosan
111 polymer chains association (Burns et al., 2015). As for the photodynamic properties of PS-

112 modified CH film, recent literature has shown that PSs conjugated with CH chains (Shrestha &
113 Kishen, 2012) or saccharide like-structures (Cellamare, Fini, Agostiano, Sortino & Cosma, 2013)
114 retained their photoactive properties making it a possible option for PDT applications. On the
115 other hand, only one paper by P. Mandal and co-workers (Mandal, Manna, Das & Mitra, 2015),
116 was known in literature related to Chl*a* molecules and chitosan hydrogel as scaffold, for
117 application in artificial light harvesting antenna. In this paper, stacked Chl*a* molecules were
118 entrapped within the chitosan matrix, then the pigment is not in its monomeric form and it is not
119 photoactive (Mandal et al., 2015).
120 Starting from these considerations a comprehensive investigation on the CH/CD/Chl*a* film
121 properties has been thus undertaken in our laboratories using several complementary techniques,
122 namely spectroscopic, calorimetric, X-ray diffraction analyses and microscope imaging methods.
123 A comparison of Chitosan biofilms arisen from our innovative procedure (with and without CD)
124 with those well characterized in literature and arisen from a well-known procedure have been
125 also performed in order to strengthens similarity and differences between them. In addition, for
126 the first time, in order to show the photoactivity of the hybrid system CH/Chl*a*, among ROS,
127 Singlet Oxygen is searched for. Nanosecond laser flash photolysis technique provides evidence
128 for the population of the excited triplet state of Chl*a* and the photogeneration of singlet oxygen is
129 demonstrated by both direct detection by using infrared luminescence spectroscopy and chemical
130 methods based on the use of suitable traps. The main results arising from such characterization
131 involving Chl*a* in solid state device will be described in the present paper opening new horizons
132 in an enhanced antimicrobial activity of chitosan film for possible applications in PDT.
133 **2. Experimental Section**
134

2.1 Materials

All the chemicals used were of analytical grade and samples were prepared using double-distilled water. Commercial grade Chitosan powder (CH, from crab shells, with a molecular weight of 150000, highly viscous, with a hypothetical deacetylation degree ≥ 75%), Acetic acid (99,9 %), EtOH (99,9 %) and glycerol (99,9 %) were purchased from Sigma Aldrich.

The deacetylation degree has been experimentally estimated. Among several methods proposed for measuring the real degree of acetylation, DS(Ac), of CH, ^{1}H-NMR (700 MHz) and FTIR-ATR analyses have been used.

As for this purpose, Equations 1 and 2 have been used for NMR and IR obtained data, respectively (Kasaai, 2008; Baxter, Dillon, Taylor & Roberts, 1992; Lavertu et al., 2003). Chitosan powder (1% v/v) was dissolved in D_2O and deuterated acetic acid (0.8% v/v) medium for NMR analysis and trimethylsilyl-propionic-2,2,3,3-d4 acid, (TSP), has been used as a references. Conversely, for FTIR-ATR ones, CH STD solid state film was directly analysed.

$$DS(Ac)\ \% = \left(1 - \left(\frac{1}{3} H_{Ac} / \frac{1}{6} H_{26}\right)\right) x\, 100$$

Equation 1

$$DS(Ac)\ \% = \left[100 - \left(\frac{A_{1637}}{A_{3450}}\right) x\, 115\right]$$

Equation 2

H_{Ac} (δ2.50 ppm) and H_{26} (δ4.20 ppm) represent the calculated experimental integrals of the indicated protons and, A_{1637} and A_{3450} represent the intensity of the IR signals at indicated wavenumbers (see FTIR-ATR section for the assignment of the vibration modes) also corrected with baselines proposed in literature (Baxter et al., 1992).

Not surprisingly, NMR and IR results were agreed between them, giving a DS(Ac) % around 30 % confirming the manufacturer's Sigma Aldrich specification. Chl*a* was extracted and purified from spinach leaves using Omata and Murata method (Omata & Murata, 1980) whose details can be found in Supplementary Material.

Chl*a* stock solutions were stored in acetone at -80°C. 2-HP-β-CD was purchased from Fluka and used without further purification.

2.2 Procedure for CH film preparation

We propose the same procedure recently applied by some Authors of this paper (Rizzi et al., 2014). CH powder was dissolved in 0.1% (v/v) aqueous acetic acid solution, in order to obtain a 2% (w/v) of Chitosan, by constant continuous stirring for 24 hrs to obtain an homogeneous solution. 200μL of glycerol were added every 100 mL of CH acetic solution. Then, the solution was filtered through a coarse sintered glass filter due to the great amount of CH not dissolved and degassed for 1 hr. The reduced acetic acid amount and the excess of CH ensures the neutral pH occurring to be 6 unit. After degassing, the CH solution was poured into a plastic Petri plate. The latter was maintained in an oven at 60˚C for 24 hrs. A thin (CH) membrane was obtained. The same procedure was followed to obtain (CH/CD) films modified with 2-HP-β-CD used as a cross-linker. In particular, the 2-HP-β-CD powder was added to chitosan hydrogel obtaining a solution having a final concentration of 10^{-3} M.

The difficulty of incorporating water insoluble Chl*a* molecules in CH/CD films has been circumvented by means of the casting technique from EtOH solution: 2×2 cm squared pieces of CH/CD free standing films were soaked with an EtOH solution containing Chl*a* (10^{-3}M) at 25 °C for 24 hrs resulting in a successful entrapment of the pigment inside the

as prepared films. The outer surface of CH/CD/Chl*a*-modified films were washed with double-distilled water and air-dried before performing any characterization. All samples have been analysed at least in triplicate. The amount of Chl *a* loaded inside the CH/CD film was 0.12 ± 0.02 g/cm^2, obtained evaluating the difference between the amount of Chl*a,* presents in EtOH solution, before and after the adsorption on CH/CD film.

2.3 X-ray Photoelectron Spectroscopy (XPS) analysis.

XPS analyses were performed using a Thermo Electron Theta Probe spectrometer equipped with a monochromatic Al Ka X-ray source (1486.6 eV) operated at a spot size of 300 μm corresponding to a power of 70 W. Survey (0–1400 eV) and high resolution (C1s, O1s, N1s and Mg1s) spectra were recorded in FAT (fixed analyzer transmission) mode at pass energy of 200 and 100 eV, respectively. All spectra were acquired at a take-off angle of 37° with respect to the sample surface. Charge compensation was accomplished by a low energy electron flood gun (1 eV). Special care was devoted during the analysis to verify that no change in the samples was induced by exposure to the X-ray beam and the electron flood gun. XPS analysis was repeated on three different spots for each sample. Charge correction of the spectra was performed by taking the hydrocarbon (C-C, C-H) component of the C1s spectrum as internal reference (binding energy, BE = 285.0 eV). Atomic percentages were calculated from the high resolution spectra using the Scofield sensitivity factors set in the ThermoAvantage V4.87 software (Thermo Fisher Corporation) and a non-linear Shirley background subtraction algorithm. The best-fitting of the high-resolution XPS spectra was performed using with mixed Gaussian-Lorentzian peaks after a Shirley background subtraction; a maximum relative standard deviation of 10% was

200 estimated on the area percentages of the curve-fitting components, while the determined standard
201 deviation in their position was ± 0.2 eV.
202
203 **2.4 Differential Scanning Calorimetry (DSC).**
204 DSC measurements were performed with a Q200 TA Instruments thermal analyzer calibrated
205 with indium as standard.
206 For thermogram acquisition, sample sizes of 1 to 2 mg were scanned with a heating rate of
207 5°C/min over a temperature range from 25°C to 300°C. Dry material was placed in an aluminum
208 cup and hermetically sealed. Chl*a* samples were prepared by casting from ethanol solution in the
209 aluminum caps. Empty cup was used as a reference and runs were performed in triplicate.
210 Samples were analyzed under continuous flux of dry nitrogen gas (50 mL/min).
211
212 **2.5 UV-Visible and FTIR-ATR spectroscopic measurements.**
213 UV-Vis absorption spectra were recorded using a Varian CARY 5 UV-Vis-NIR
214 spectrophotometer (Varian Inc., now Agilent Technologies Inc., Santa Clara, CA, USA). FTIR-
215 ATR spectra were recorded within the 600–4000 cm^{-1} range using an Fourier Transform Infrared
216 spectrometer 670-IR (Varian Inc., now Agilent Technologies Inc., Santa Clara, CA, USA),
217 whose resolution was set to 4 cm^{-1}. 32 scans were summed for each acquisition.
218
219 **2.6 Water Vapor Transmission Rate (WVTR).**
220 WVTR of CH based materials was evaluated using 7002 Water Vapour Permeation Analyzer
221 (Illinois Instruments, Inc. U.S.). The instrument displays the WVTR as either g/m^2/day or
222 g/100in2/day and into the instrument is incorporated a Pb_2O_5 sensor. According to the Faraday's

Combined Laws of Electrolysis, the electrolytic current is a measure of the rate at which water is electrolyzed. Under equilibrium conditions this equals the rate at which moisture is being absorbed by the Pb_2O_5 film. Thus, knowledge of the gas flow rate through the housing and the current in the cell gives an absolute measure of the moisture contained in the sample gas. The films were stored in the cell at 25 ± 1 °C and 90 ± 1% relative humidity (RH) for 24 hrs.

2.7 Scanning Electron Microscopy (SEM).

The surface morphology of the CH, CH/CD and CH/CD/Chl*a* films was investigated using a Zeiss SUPRA™ 40 field emission scanning electron microscope (FE-SEM). SEM images were acquired with a conventional Everhart-Thornley detector at the working distance of 5 mm and electron acceleration voltage of 0.6 kV.

2.8 Atomic Force Microscopy (AFM).

AFM experiments were performed by a PSIA XE-100 SPM system in AFM mode, and cantilevers with silicon nitride tips were used. Topography images were recorded in non-contact mode at a 1 Hz scan rate with a resolution of 512 × 512 pixels.

2.9 X-ray diffraction (XRD).

X-ray diffraction data were collected at room temperature from CH standard, CH, CH/CD, CH/CD/Chl*a* and CH/CD in EtOH films Measurements were performed at a fixed incident angle of 3° by a Bruker D8 Discover diffractometer, equipped with a Göbel mirror, using Cu Kα radiation ($\lambda_{K\alpha1}$ = 1.54056 Å and $\lambda_{K\alpha2}$ = 1.54439 Å), and a scintillation detector. The working

conditions were set to 40 kV and 50 mA. Data were collected in the range 5–60° with a step size of 0.1°.

2.10 Laser flash photolysis setup.

The sample was excited with the third harmonic of a Nd–YAG Continuum Surelite II–10 laser (355 nm, 6 ns, ~ 10 mJ). The quartz plate with the chitosan-based film was aligned at an angle of 45° with respect to both the excitation and the monitoring beams. The reflection of the excitation from the quartz plate was to the opposite side of the transient signal detection. The measurements in solution were carried out with a 10 × 10 mm^2 quartz cell with a 3 mL capacity. The excited sample was analyzed with a Luzchem Research mLFP–111 apparatus with an orthogonal pump/probe configuration. The probe source was a ceramic xenon lamp coupled to quartz fiber-optical cables. The laser pulse and the mLFP–111 system were synchronized by a Tektronix TDS 3032 digitizer, operating in pre-trigger mode. The signals from a compact Hamamatsu photomultiplier were initially captured by the digitizer and then transferred to a personal computer, controlled by Luzchem Research software operating in the National Instruments LabView 5.1 environment. The sample temperature was 295 ± 2 K. The energy of the laser pulse was measured at each shot with a SPHD25 Scientech pyroelectric meter.

2.11 Direct detection of $^1O_2$.

Steady-state emission of $^1O_2$ in the NIR region was recorded with a Fluorolog-2 Mod-111 spectrometer, equipped with a InGaAs detector maintained at –196 °C, by illuminating the film sample, immersed in a quartz cuvette filled D_2O and placed at 45° with respect the excitation beam, with a 405 nm CW laser (2 W cm^{-2}).

2.12 Photoactivity measurements.

In order to demonstrate the photoactivity of chitosan film containing Chl*a*, direct and indirect methods were employed to achieve our aim. 4-thiothymidine (S^4TdR, Carbosynth Limited, UK) and Singlet Oxygen Sensor Green (SOSG, Molecular Probes, Inc. by Life Technologies Limited, Scotland) have been used in aqueous solution at concentration of 10^{-5} M and 1.5 μM, respectively. These aqueous solutions containing a slice film 1×1 cm were illuminated with a neon lamp, whose emission had been previously assessed to occur mainly between 400 and 700 nm and with a power surface density of 60 mW/cm^2. The solution absorption or emission spectra were recorded at different times of irradiation. S^4TdR absorption spectra were recorded in the range of 200-800 nm (λ^{max} = 337 nm in aqueous solution and 326 in D_2O). SOSG emission was registered at 525 nm (λ_{ex} = 488 nm). Its maximum absorption peak was at about 500 nm. Chitosan film containing-Chl*a* absorption spectra were recorded in the range of 350-800 nm.

As far as SOSG, it is reported in literature (Cellamare et al., 2013) as a highly selective singlet oxygen fluorescent probe with a fluorescein moiety bound to an anthracene derivative. The reaction with singlet oxygen increases the observed emission at 525 nm due to the generation of an endoperoxide specie as a main product. A 550 nm cut-off glass filter has been used to reduce the self-production of $^1O_2$ by SOSG. Measurements were achieved before irradiation and every 10 minutes for 100 minutes. As far as S^4TdR is concerned, it is a modified nucleoside able to react with singlet oxygen without, at moment, selectivity in the presence of ROS. Moreover our recent studies show its high photostability, if solution was irradiated with visible light (Rizzi et al., 2014). Measurements were achieved before irradiation and after 100 minutes.

As far as the irradiation of Chitosan film-containing Chl*a*, it has been realized, directly, with a slice film (1×1 cm) putted on neon lamp, and UV-Visible absorption-measurements have been performed before irradiation and every 10 minutes for 100 minutes employing a supporting film-device. The fluorescence measurements were conducted using a spectrofluorimeter Varian CARY Eclipse 68. A quartz cuvette with an optical path length of 1 cm has been employed for all spectroscopic measurements.

3. RESULTS AND DISCUSSION

3.1 UV-Vis spectroscopy analysis.

As already known (Ryan & Senge, 2015), the molecular structure of Chl*a* shows typical features: the heteroaromatic character of the porphyrin system, the central metal and a long chain made of carbon atoms (Ryan & Senge, 2015). As a preliminary study based on UV-Vis spectroscopy, the spectrum (350−800 nm) of polysaccharide film, CH/CD, containing Chl*a* (CH/CD/Chl*a*), entrapped by soaking in an ethanolic solution, was acquired and reported in Figure 1a. The camera picture of a large sample CH/CD/Chl*a* is reported in Figure 1 showing the homogeneous distribution of Chl*a* inside the film. At first glance, a characteristic Chl*a* absorption spectrum is clearly observed. The spectrum is characterized by an intense Soret band at about 422 nm, in the blue region of the visible spectrum, and a $Q_Y(0,0)$ band, in the red region, at about 663 nm (Manna, Basu, Mitra & Mukherjee, 2009; Omata & Murata, 1980). In accordance with our experience and by comparing the spectrum showed in Figure 1a with one recorded in alcoholic solution and reported in Figure 1b, (in which the Chl*a* occurs in its monomeric and photoactive form),

313 it is evident that inside the CH/CD film (Figure 1a) the pigment maintains its active form
314 (Agostiano et al., 2003; Agostiano et al., 2002a; Dentuto et al., 2007). Interestingly, a
315 detailed observation of the absorption spectrum reveals a significant ipsochromic shift of
316 the Soret band (from 430 nm in alcoholic solution to 419 nm in CH/CD film), which
317 appears unstructured, broadened and also characterized by a hyperchromic effect. In
318 addition, a slight blue shift of the $Q_Y(0,0)$ band was revealed if compared with the same
319 band recorded in the ethanolic solution (Figure 1b). It is worth mentioning that the
320 spectral differences can be better observed by means of the first derivative analysis of the
321 UV-Vis absorption spectrum of the CH/CD/Chl*a* film (Figure 1a, inset). The Soret band
322 indicates the presence of two spectral components located at 403 and 430 nm,
323 respectively. More specifically, the two latter correspond to different conformations and
324 orientations of the Chl*a* porphyrin macrocycle inside the film.
325 These results suggest that different interactions between Chl*a* and CH/CD-composite film
326 were established, involving a change in chitosan chains coordination due to the symmetry of
327 Chl*a*-porphyrin ring in chitosan film (Mandal et al., 2015).
328 Accordingly, also the first derivative analysis performed on the absorption band located at 661
329 nm shows the presence of two spectral components ascribable to different forms of the pigment:
330 (i) a monomer form and (ii) a hydrated dimeric one (Agostiano et al., 2003; Agostiano et al.,
331 2002a; Dentuto et al., 2007) represented by signals located at 649 nm and at 675 nm,
332 respectively (Agostiano, Catucci, Colafemmina & Scheer, 2002). Comparable wavelength values
333 were also reported in literature, for Chl*a* solubilized in aqueous surfactants solutions and in
334 water–organic solvent mixtures (Agostiano et al., 2002a, b; Agostiano, Cosma, Della Monica &
335 Fong, 1990; Agostiano, Catucci, Colafemmina & Della Monica, 1996; Agostiano, Cosma &

Della Monica, 1991; Agostiano, Cosma, Trotta, Monsù-Scolaro & Micali, 2002), proving our considerations . More specifically, the interaction of Chl*a* with positive charges, able to induce a blue shift of the Q_Y band together with the lack of resolution of the Soret band at 419 nm (Agostiano et al., 2002b) was suggested. Additionally, such observed broadening, at 419 nm, can be related to strong interactions between Chl*a* and Chitosan chains (Mandal et al., 2015). In conclusion the spectral components located at 675/430 nm indicate the interactions between CH/CD and Chl*a* *via* water molecules (Mandal et al., 2015; Agostiano et al., 2002b; Agostiano et al., 1990; Agostiano et al., 1996; Agostiano et al., 1991; Agostiano et al., 2002a; Chauvet, Viovy, Santus& Land, 1981), while those located at 403/649 nm suggest the interactions with positive charged (Mandal et al., 2015; Ryan &Senge, 2015; Agostiano et al., 2002b) amino groups present on CH chains.

In order to draw more detailed information on the interactions leading to the generation of CH/CD/Chl*a* blended film, and to gain insights into the surface chemical composition of the blended films prepared in this work, XPS analyses were carried out on the CH film produced with the new procedure after immersion in ethanol, the CH/CD film after immersion in EtOH and the CH/CD/Chl*a* film.

In order to evidence only similarities and differences between CH STD and CH or CH/CD, and thus to show the property of the latter, from now and when it was necessary for a question of clarity, the results related to CH STD have been reported every time.

3.2 XPS analysis.

XPS atomic percentages are reported in Table S2, while the high-resolution XPS C1s and N1s spectra and the summary of the curve-fitting results are shown in Figure 2 and Table 1, respectively.

The C1s spectrum of the CH film, prepared by means of our novel procedure, (Figure 2a) is curve fitted with four peaks (Beamson & Briggs, 1992; Roy, Samanta, Mukherjee, Roy & Mukherjee, 2013; Kang, Liu, Zheng, Qu & Chen, 2010): the hydrocarbon component at 285.0 eV (C1, 30%) due to adventitious hydrocarbon contamination and to a possible contribution of methyl groups of acetate anions, the most abundant component at 286.5 eV (C2, 56%) ascribed to both C-N and C-O groups present in the chitosane polymer, the peak at 288.1 (C3, 13%) assigned to both N-C=O groups in N-acetylglucosamine units and O-C-O moieties, the very weak peak at 289.1 eV (C4, 1%) due to carboxylate groups of acetate anions. The N1s spectrum is composed by a principal component at 399.7 eV, ascribed to both unprotonated amino and amide groups (N2, 93%), and a second weak component at 401.5 eV associated to protonated amino groups (N3, 7%) (Roy et al., 2013; Kang et al., 2010).

No significant variations are observed in the XPS C1s and N1s signals when 2-HP-β-CD is present in the film (Figure 2b), in fact, comparable curve-fitting results are obtained for CH and CH/CD films. On the other hand, the presence of Chl*a* in the CH/CD/Chl*a* film induces a remarkable variation of the XPS C1s signal (Figure 2c); in particular the considerable increase of the peak area percentage of the hydrocarbon component at 285.0 eV can be ascribed to Chl*a* and, specifically, to contributions from the phytyl chain, aromatic carbon atoms of the porphyrinic ring, alkyl and alkenyl substituents of the porphyrinic ring. Noticeably the N1s spectrum of the CH/CD/Chl*a* film shows a new component at 398.3 eV attributed to nitrogen atoms in the Chl*a* porphyrin macrocycle (Brace et al., 1978; Karweik & Winograd, 1976; Bekalé, Barazzouk &

Hotchandani, 2012a; Bekalé, Barazzouk & Hotchandani, 2012b). Interestingly, the ratio between the peak area percentages of the N3 (NH_3^+) and N2 (NH_2/N-C=O) components increases from 0.075, as observed for both CH and CH/CD films (N2 and N3 peak percentages of 93% and 7%, respectively), to about 0.12 in the case of the CH/CD/Chl*a* film (N2 and N3 peak percentages of 78% and 9%, respectively); this confirm, in excellent agreement with the so far discussed hypothesis, a rearrangement of the CH chains induced by Chl*a* incorporation suggesting a novel disposition of the protonated amino groups on the film surface arising from novel coordination as well suggested by Mandal (2015).

3.3 Differential Scanning Calorimetry.

Additional information on CH, CH/CD and CH/CD/Chl*a* films was searched for through DSC analysis. It was ascertained in literature that polysaccharides show strong affinity for water and in the solid state a disordered structures that can be easily hydrated has been already proposed (Harish Prashanth, Kittur & Tharanathan, 2002; Pereira Jr., Queiroz de Arruda & Stefani, 2015). Indeed, calorimetric studies on analogue systems indicate a weight loss, from polymer, in four consecutive steps. The first two steps (endothermic) are due to the loss of surface water from biofilm; the third and fourth ones (exothermic) are due to the decomposition process (Pereira et al., 2015) of the acetylated and deacetylated units of the polymer and its cracking (Pereira et al., 2015; Kittur, Prashanth, Sankar & Tharanathan, 2002).

The main DSC curves related to CH, CH/CD and CH/CD/Chl*a* films are showed in Figure 3 and a comparison has been undertaken also with Chl*a* samples prepared by casting from ethanol solution in the aluminum caps (Figure 3a).

CH film thermogram, in agreement with what reported in literature (Pereira et al., 2015; Kittur et al., 2002) for the well-known CH STD, displays an endothermic phase (from 40°C to 150°C), due to the evaporation of water, and an exothermic phase (in the range 240°C-300°C) due to Chitosan degradation (Figure 3b).

Interestingly, looking all thermograms, differences in the endothermic peak areas and positions have been observed indicating different water-polymer interactions (Harish Prashanth et al., 2002).

More specifically, the presence of CD in CH films produces a slight shift of the first broad endothermic peak associated to the loss of water towards lower temperature and a decrease in its area (Figure 3c). In other words CH film containing CD shows lower hydrophilic character likely due to a different organization of polymeric chains. The less amount of water in the latter indicates a weaker interaction of water with films, leading a lower evaporation temperature. Not surprisingly, in accordance with Prashanth and co-workers (Harish Prashanth et al., 2002) the presence of CD does not induce any important changes in the peak associated to the degradation process (Karweik & Winograd, 1976). As for the EtOH effect on CH/CD film, the thermogram (Figure 3d) reveals that such film occurs with more pronounced hydrophobic properties than the same previous the treatment (Figure 3c). This is also confirmed by the clear lower amount of withheld water induced by the alcoholic dehydrating action. Additionally, the film occurs to be more stable than the CH and CH/CD ones.

On the other hand the incorporation of Chl*a* in CH/CD films (Figure 3e) produces an opposite effect on the endothermic and exothermic peaks, associated respectively to water loss and film decomposition. The first one is shifted to lower temperature whereas the second one is moved

424 towards higher temperature values. Thus the pigment makes films less hydrophilic and more
425 stable than CH and CH/CD ones.
426 In addition, in the thermogram of CH/CD/Chl*a* film the melting peak of Chl*a* is not visible
427 (Figure 3a and 3e). It could be due to the presence, in the same temperature range, of the broad
428 endothermic peak associated to the loss of water and/or to an absence of the melting pigment
429 peak which should indicate that the pigment in such condition is present in an amorphous state.
430 In conclusion the further observed decrease in film affinity towards water due to presence of
431 Chl*a* in CH/CD films was in agreement with those expected considering the hydrophobic
432 character of the Chl*a* molecule. Differently, the increased film stability (film composition
433 temperature occurs higher than 250 °C) is noteworthy since Chl*a* is not stable at such
434 temperature. Thus, the presence of Chl*a* induces a reorganization of polymeric chains in the
435 films affecting the thermal degradation process and as already explained in literature (Pereira Jr.
436 et al., 2015; Kittur et al., 2002) such effect can be attributed to variation induced on amino group
437 of chitosan chains. Results once again suggest the main role of Chitosan amino groups in Chl*a*
438 and CH/CD film interactions.
439
440 **3.4 FTIR-ATR spectroscopy measurements.**
441 In order to better understand the molecular organization of Chl*a* inside the CH/CD composite
442 film, and thus detailing previous showed measurements, FTIR-ATR analyses were performed on
443 CH film arising from the known standard procedure, CH film prepared with the new method,
444 CH/CD and, last but not least, on CH/CD/Chl*a* films. Although similar to each other as a whole,
445 FTIR spectra show slight differences in the absorption intensities and peak positions.

For the sake of comparison, in Figure 4d, the FTIR spectra of CH STD (black line) and CH films (grey line) are reported, showing analogies and differences between the two different typologies of films. Thanks to previous studies related to chitosan films, it is possible to individuate the characteristic IR bands of CH in our condition: in the 3300-3400 cm^{-1} range (N-H, 3276 cm^{-1}, and O-H, 3346 cm^{-1}, stretching), the doublet (2923/2875 cm^{-1}) relative to the symmetric and asymmetric C-H stretching in the 2700-3000 cm^{-1} range, the amide I band (-NHR-CO- stretching) at 1637 cm^{-1} and at 1550 cm^{-1} there is the overlapping of the signal relative to the NH_2 bending (amide II) of chitosan with the carboxylate stretching vibrations of acetate anions, which presents also a signal at 1410 cm^{-1}. Bands occurring at 1151 cm^{-1} and 1059 cm^{-1} due to the C-O-C asymmetric and symmetric stretching, respectively, and at 1031 cm^{-1} due to the C-O stretching of the alcoholic moieties, are known to be typical for saccharide structure (Synytsya, Grafová, Slepicka, Gedeon & Synytsya, 2012; El-Hefian, Nasef & Yahaya, 2012; Liu, Adhikari, Guo & Adhikari, 2013).

In general, for all spectra reported in Figure 4 it is evident the absence of narrow absorption bands around 3300 cm^{-1} indicating the absence of free OH groups, conversely the occurrence, as expected, of intra and intermolecular hydrogen bonds were proposed in such condition in accordance with similar studies reported in literature (Burns et al., 2015). The region above 3000 cm^{-1} presents slight differences in the O-H and N-H band position and a shift to higher wavenumbers, from 3346/3276 cm^{-1} in the standard CH film to 3353/3294 cm^{-1} in the CH film containing Chl*a* and 2-HP-β-CD (Figure 4a, d), indicating an increase of more ordered structures (Thakhienw, Devahastin&Soponronnarit, 2013 and reference therein). By comparing the two IR spectra referred to CH film prepared in accordance with standard (Figure 4d, black line) and new method (Figure 4d, grey line), at a first glance it is possible to observe that the neutral CH film

presents the amide I band (carbonyl band) and the amide II band (bending of the aminic group) shifted to higher wavenumbers (the first one shifts from 1637 cm^{-1} to 1653 cm^{-1}, the second one from 1550 cm^{-1} to 1560 cm^{-1}). Moreover, the intensity ratio between the two bands appears reversed if the neutralized film (CH film) is considered. It is well known that these signals, as well the hydrogen bonding formation, are sensitive to the chitosan acetylation degree (DS(Ac)) and to the organic acid used for film preparation (El-Hefian et al., 2012; Liu et al., 2013; Thakhienw et al., 2013; Nunthanid, Puttipipatkhachorn, Yamamoto & Peck, 2001; Chen et al. 2011).

In particular the intensity of amide I signal decreases as a function of the DS(Ac), disappearing in completely deacetylated chitosan (Kasaai, 2008), whereas the amide II band shifts to higher wavenumbers (Harish Prashanth et al., 2002). In our case the standard CH film spectrum (black line), which contains a greater amount of acetic acid (see Experimental Section), reveals that the signal relative to the protonated aminic group $-NH_3^+$ and generally present as a shoulder at about 1514 cm^{-1}, is completely absent (Demarger-Andre & Domard, 1994). This indicates that the acetic acid carboxylates interact ionically with positively charged amino groups on the CH chain reducing the amount of free amino groups as if the DS(Ac) of CH is lowered (Chen et al., 2008). Thus the inversion of the intensity ratio in the neutralized film is indicative of a reduced amount of acetate anion, which is unable to act as electrostatic cross-linker between the chitosan chains making less intense the mediated interchain interactions. This hypothesis is also confirmed by the narrowing and intensity increasing of the O-H and N-H stretching band and by the shift of the related wavenumbers indicative of a greater mobility (Burns et al., 2015). The addition of 2-HP-β-CD (Figure 4c, gray line) to CH film essentially induces changes in the band positions which shift slightly to lower wavenumbers as a whole. In fact in general CD and chitosan are

492 characterized by similar FTIR signals, but as 2-HP-β-CD amount is lower than CH one, the
493 effect of the CD presence is evidenced by slight changes of the wavenumbers of CH spectral
494 bands. Interestingly, in presence of CD, due to the great amount of O-H groups, the O-H and N-
495 H stretching band, if compared with the same one without CD (see Figure 4c, black line), occur
496 broadened and slightly shifted at lower wavenumber indicating the involvement of both inter-
497 and intramolecular hydrogen bonds between CH chains and cyclodextrin ones (Chen et al., 2008;
498 Bostan et al., 2014). These results are not surprising, in fact it was well know that CDs addition
499 promotes chitosan polymer chains association (Burns et al., 2015). The C-H symmetric and
500 asymmetric stretching (CH STD) shifts to higher wavenumbers: from 2923 to 2938 cm^{-1} and
501 from 2875 to 2881 cm^{-1}, respectively. In particular these displacements could be also indicative
502 of non-polar intermolecular interactions between CD and CH chains (Harish Prashanth et al.,
503 2002). Amide I (1653 cm^{-1}) and the $-NH_2$ (1560 cm^{-1}) signals are very intense with the ratio
504 again inverted. Furthermore, it is present a signal at 1410 cm^{-1} indicative of the presence in the
505 CD-modified CH film of a greater amount of acetate anion as regards of the neutralized film
506 without 2-HP-β-CD. This could be attributed to a greater difficulty in the acetic acid removal
507 from the film due to the presence of cyclodextrin. This interaction between acetic acid/CD and
508 CH is confirmed also by the bands in the region characteristic of glucopyranose (1100-900 cm^{-1})
509 which appear more intense and broader indicating non-polar interaction between CH chains and
510 cyclodextrin ring (Wang et al., 2007). In general in the case of salts involving aminic groups the
511 presence of strong hydrogen bonds determines an increase of the intensity and a broadening of
512 the IR N-H signals together with a frequency lowering (Jug, Maestrelli & Mura, 2012). For the
513 CH film containing CD this situation is due to the 2-HP-β-CD ability of forming hydrogen bonds
514 which increments the CH interchain distance allowing a higher penetration of the acetate anion

515 which in turn interacts electrostatically with CH as shown by the absence of the signal relative to
516 the $-NH_3^+$ group at about 1514 cm^{-1}.

517 Since the insertion of Chl*a* in the film has been obtained by dipping the CH film in an
518 ethanolic solution containing the pigment, it has been evaluated the effect of the immersion of
519 the film in ethanol. In the Figure 4b the comparison between the CH film with CD before and
520 after the immersion in ethanol was showed. Clearly the contact with EtOH generates a novel
521 disposition of CH chains, shielding them from detection (Burns et al., 2015) which results in a
522 reduced absorption intensity of the film as a whole. This could be indicative of the presence of
523 strong interactions due to additional interchain hydrogen bonds that partially block vibrational
524 modes (Coates, 2000). This result is similar to the one obtained for CH STD (Figure 4d), in
525 which strong inter and intra chain interactions were established. Further signals appear at 2925
526 $cm^{-1}$and at 879 cm^{-1} ascribable to the EtOH presence in the film inducing chitosan chains
527 rearrangement (Jug et al., 2012; He, Ao, Gong & Zhang, 2011). In particular the ethanolic C-H
528 stretching signal is localized at 2977 cm^{-1} and it predominates over the C-H stretching signal of
529 the CH/CD system. This indicates that the film treatment with EtOH, dehydrating agent,
530 determines the removal of the acetate anion, in accordance with literature (Coates, 2000), and
531 residual water with the insertion of ethanol molecule in the formation of more extended
532 hydrogen bonds, compacting the film. These added inter-chain interactions make more rigid the
533 film vibrational mode (Coates, 2000 and reference therein). This is also confirmed by changes in
534 the CH amide and amine signals in the region 1500-2000 cm^{-1}. More specifically, amide I signal
535 shifts to 1657 cm^{-1}, while the aminic band shifts to 1571 cm^{-1} inverting their ratio. Moreover the
536 acetate anion signal at 1410 cm^{-1} disappears.

The addition of Chl*a* in the CH/CD film does not evidence new bands or substantial modification in the position of film characteristic signals (Figure 4a). The absence of the typical Chl*a* vibrational modes can be due, as expected, to the excess of chitosan and especially to the strong interactions between chitosan chains and Chl*a* restricting the vibrational mode of the latter (Mandal et al., 2015). On the other hand, it is possible to observe slight variations essentially due to disappearing of ethanol signals which determines a general intensity decrease of FTIR spectrum. The disappearance of the ethanolic signals induces a structural rearrangement of the film which results in a more compact structure. In fact in the range 2700-3000 cm^{-1}, typical of the C-H stretching, it is observed an inversion in the peaks intensity (Figure 4a, gray line). Further, the signals in the 1200-1500 cm^{-1} range, typical of saccharides, are subject to slight shifts of wavenumbers indicating a hydrogen bonding reorganization (Stuart, 2004). Also, the region below 900 cm^{-1} occurs changed indicating the contribute of the typical vibrational mode of Chl*a*-pyrrol ring (Mandal et al., 2015). Amide I and amine signals (region 1500-1800 $cm^{-1,}$ Figure 4a) present again an intensity inverted ratio. All these changes can be interpreted, in agreement with showed UV-Vis absorption spectroscopy results, considering that Chl*a* interacts with CH/CD rearranging the polymer chains association specifically involving the chitosan-amino groups. In accordance with several observations reported in literature (Cellamare et al., 2013; Mandal et al., 2015; Omata & Murata, 1980), it is possible to assume a coordination between the cationic NH_3^+ group presents on the CH chain and Chl*a* macrocycle (Mandal et al., 2015). In order to confirm these hypotheses arising from spectroscopic and calorimetric techniques additional information were searched for through Water Vapor Transmission Rate investigation.

560 **3.5 Water Vapor Transmission Rate (WVTR).**

561 WVTR of CH-based composite films with 2-HP-β-CD and Chl*a* are reported in Figure S2. The
562 effect due to the standard procedure modification necessary to prepare CH films has been also
563 evaluated. As expected the incorporation of different molecules from chitosan, and the
564 modification of the procedure to prepare CH films induces changes on the WVTR. Indeed by
565 comparing results related to CH films and CH STD one, reported in Figure S2, WVTR appears
566 in the former to be around 800 g/m^2/day, in the latter around 550 g/m^2/day. Thus, the
567 modification introduced by changing the film preparation procedure induces an increase of about
568 48% in the WVTR values. On the other hand, the addition of 2-HP-β-CD results in a WVTR
569 decrease, *i.e.* around 250 g/m^2/day (about a decrease of 70% respect to CH film and 55% respect
570 to CH standard films).

571 These results, as showed also by FTIR-ATR and DSC analysis, evidence a negative impact of
572 film modification on the WVTR due to the presence of novel chitosan chains arrangement inside
573 neutralized CH films if compared with CH STD one, allowing the transmission of water
574 molecules (Philippova, Volkov, Sitnikova & Khokhlov, 2001).

575 Always in accordance with FTIR-ATR analysis, the presence of 2-HP-β-CD induces the
576 condensation of counterions on the charged groups of polymer chains, reducing the positive
577 charge of macromolecules. The latter process induce the aggregation of chitosan chains (Xua,
578 Kimb, Hanna & Nag, 2005). About this aspect, Demarger-Andre *and co*-workers (1994) show
579 that the water content in CH films is related to the amount of NH_3^+ groups and their
580 neutralization (from NH_3^+ in NH_2) makes the film less hygroscopic than those obtained as
581 prepared (Chen et al., 2008). In our case, according to FTIR data, it seems that the acetate ion
582 plays a similar role forming ion pairs with protonated amino groups of CH chains, thus affecting

583 the hydrophobic character of CH films changing the WVTR through the films. This could be
584 attributed (Xua et al., 2005) to the difficulty in acetate ion removal in presence of 2-HP-β-CD
585 confirmed also by FTIR-ATR analysis. The same decrease in WVTR was observed after the
586 treatment with EtOH (see Figure S2) attributable to the dehydration effect of the organic
587 molecule. In particular the hydrophilic CH chains interactions are removed in order to form a
588 more stable ones with the elimination of water channels. For CH/CD films, the effect of EtOH
589 treatment is a WVTR decreasing of 80% compacting CH structure by inducing novel H-bonds
590 arrangement and improving the intrinsic hydrophobic property of CH/CD films (Coates, 2000).
591 The introduction of Chl*a* in CH/CD films (Figure S2) reduces even more the WVTR due to the
592 hydrophobic character of Chl*a* that prevents water molecule diffusing through the film and to the
593 coordination of protonated amino groups by the pigment (Coates, 2000). Both these effects
594 induce the formation of hydrophobic interactions. These results were in accordance with XPS,
595 DSC and FTIR data in which the Chl*a* presence induces arrangement on chitosan chains in
596 which the NH_3^+ groups are involved.
597
598 **3.6 SEM analysis.**
599 SEM images reported in Figure S3 show that the CH films prepared with the standard
600 (Figure S3a) and the new procedure (Figure S3b) have a similar morphology, *i.e.*, the
601 films are homogeneous and smooth, however they present some protruding nodules. The
602 same results have been obtained for CH/CD film (data not shown). The overall
603 morphology of the CH film prepared with the new method and also with the standard one
604 (data not shown) does not change significantly after immersion in ethanol (Figure S3c),
605 however, it is worth mentioning that EtOH immersion seems to slightly increase the

606 surface roughness of the films, as also observed by AFM (see section 3.7). The nodules
607 present in the CH films (Figure S3, panels b and c) disappear in the CH/CD film
608 immersed in ethanol (Figure S3d); indeed in the latter case the formation of some
609 depressions is observed (arrows in Figure 2d). Depressions seem uniformly distributed
610 over the entire surface of the sample. This evidence suggests that the incorporation of 2-
611 HP-β-CD induces changes in the arrangement and packing of CH polymer chains and,
612 therefore in accordance with our discussion, alters the surface morphology of the film.
613 The morphology of the CH/CD film does not change significantly when Chl*a* is present
614 (Figure S3e); while the homogeneity of the CH/CD/Chl*a* film indicates that a quite
615 uniform distribution of Chl*a* is obtained in the layer. Results were in accordance with the
616 clear homogenous distribution of the pigment inside the film (see picture in Figure 1).
617
618 **3.7 AFM analysis.**
619 In order to present a deepest morphological investigation, the analysis of, "as prepared" and
620 upon EtOH treatment, CH STD, CH as well as CH/CD films has been carried out by means of
621 AFM images, reported in Figure 5. Even though the films of CH STD (Figure 5a) and CH
622 (Figure 5b) show a homogeneous distribution, according to SEM analysis, the CH film appears
623 more rough (R_q = 1.5 nm) than the CH STD (R_q = 0.5 nm). Such experimental evidence could be
624 ascribed to the large amount of CH in the latter one. In particular, the hydrogen bonds are
625 believed to play an essential role in organizing the macromolecules of CH chains (Philippova et
626 al., 2001). In accordance with previous showed data, the chains organization is essentially due to
627 intra- and intermolecular interactions in the case of CH STD film (Philippova et al., 2001).

On the other hand, we suppose that at lower amount of CH chains than in CH STD, like in the case of CH film, the intramolecular interactions are present in a preponderant way, so that it shows a structure less dense compared to that one of CH STD, in which we suppose the presence of inter-domains water channels.

The introduction of CD makes more smooth the CH film, so that the R_q value decreases to 1.1 nm (Figure 5c). Likely further hydrogen bonds (Burns et al., 2015) between molecules make to rearrange the CH chains differently in a closely packed fashion. Such experimental evidence, strengthens FTIR data showing that the interactions in CH/CD films are quite similar to CH STD ones thus suggesting that H – bonds are responsible of the interactions between CH and 2-HP-β-CD (Burns et al., 2015). Such a hypothesis is further confirmed in the corresponding AFM phase images. Indeed, it is clearly evident that the introduction of CD (Figure S4b) changes notably the organization of CH film (Figure S4a) thanks to the increasing interactions between the two different materials.

For the sake of comparison of CH film with ones obtained in the presence of Chl*a*, the effect of EtOH solution on CH morphology has been also evaluated. Upon treatment, by immersing such films in EtOH, AFM topographies were recorded and showed in Figure 5d-e. First of all, an important modification in the structure of such films is observed with respect to the "as prepared" films (Figure 5a-c). It is well known that CH is insoluble in EtOH, so that a reorganization of CH chains is supposed in a favorable thermodynamic situation, in "polystyene" fashion, as reported in literature (coates, 2000) obviously due to the decrease of the polarity of medium. Moreover, while the R_q value for the CH STD film is retained, in the CH and CH/CD films treated with EtOH it is increased with respect to corresponding films before the treatment.

650 However, the trend of R_q values of CH STD, CH and CH/CD is unchanged in both cases, with or
651 without treatment with EtOH.
652 The AFM phase images of the CH (Figure S4c) and CH/CD (Figure S4d) films after
653 immersing in EtOH highlight the presence, in the latter case, of a second material represented by
654 2-HP-β-CD thanks to different color contrast of spots with respect to background of image. It is
655 clearly evident the "nanoparticle-dominant" structure of CH film treated with EtOH as proposed
656 by Qing He and co-workers (Coates, 2000). In accordance with WVTR and FTIR-ATR data, CH
657 films compact their structure in contact with EtOH inducing the formation of novel H-bonds.
658 The effect is less pronounced in CH STD since the dehydrate compact structure is poor in water
659 channel. Upon the introduction of Chl*a* in the CH/CD film a slightly increase of the R_q to 1.2 nm
660 has been observed (Figure 6a). However, the film appears quite homogeneous thus suggesting
661 that the different materials (CH, CD, Chl*a*) are distributed regularly in the film. Such
662 experimental evidence is confirmed also by AFM phase image (Figure 6b).
663
664 **3.8 X-ray diffraction results.**
665 To inspect the crystalline/amorphous nature of the chitosan-based films, X-ray diffraction data
666 have been collected on CH STD, CH, CH/CD and CH/CD/Chl*a*, since it was demonstrated in
667 literature (Coates, 2000; Xua et al., 2005; Ogawa, Hirano, Miyanishi, Yui & Watanabe, 1984)
668 that the polymorphism and crystallinity as well as the amorphous state strongly depends on its
669 preparation methods (Ogawa, Toshifume & Masaru, 1992).
670 X-ray patterns collected on both standard and modified chitosan (Figure S5) films show the
671 existence of an amorphous phase for all the investigated samples. With respect to the standard,
672 (Figure S5a) the incorporation of 2-HP-β-CD (Figure S4b) and Chl*a* (Figure S5c) as well as of

673 EtOH (Figure S5d) did not significantly affects the amorphous nature of the films based on the
674 modified chitosan (CH).
675
676 **3.9 Photoactivity studies.**
677 Photoactivity of the film containing Chl*a* was investigated by combining time-resolved and
678 steady-state spectroscopic and photochemical techniques. The excited triplet state of Chl*a* is the
679 key transient intermediate for the photosensitization of $^1O_2$ and its effective generation upon light
680 excitation is thus crucial for the photodynamic action. Laser flash photolysis with nanosecond
681 time-resolution is a powerful tool for obtaining spectroscopic and kinetic features of excited
682 triplets of porphyrinoid systems since these transient species exhibit intense absorptions in the
683 visible region and possess lifetimes falling in the microsecond time regime (Ogawa et al., 1992).
684 Figure 7 shows the transient absorption spectrum recorded 0.2 μs after 355 nm laser excitation of
685 the chitosan film containing Chl*a*. This transient spectrum shows the typical features of the
686 excited triplet state of the Chl*a* with a maximum at ca. 460 nm and a bleaching due to the Soret
687 ground-state absorption at ca. 410 nm. The triplet state decays mono-exponentially with a triplet
688 lifetime of ca. 20 μs (inset Figure 7). Furthermore, the time evolution of the absorbance changes
689 reveals that no new transient species is formed concurrently to the triplet decay.
690 Energy transfer from the triplet of Chl*a* embedded in the chitosan film to molecular oxygen
691 results in the concomitant photogeneration of $^1O_2$. Near-infrared luminescence spectroscopy is
692 the most suitable technique to unequivocally demonstrate the generation $^1O_2$. This species, in
693 fact, exhibits a typical phosphorescence signal at 1270 μm (He, Ap, Gong & Zhang, 2011). In a
694 typical experiment for $^1O_2$ detection, the film was placed in a spectrofluorimetric cuvettes
695 containing 3 mL of D_2O, and excited with a CW laser at 405 nm. D_2O was used as a solvent for

696 $^1O_2$ luminescence measurements to take advantage of the larger radiative constant and longer
697 lifetime with respect to H_2O. Figure 8 shows clear-cut evidences for the $^1O_2$ photogeneration
698 from film as proven by the characteristic luminescence spectrum in the NIR region, as result of
699 the energy transfer from the lowest excited triplet state of the porphyrin to molecular oxygen.
700 In order to demonstrate that the photogenerated $^1O_2$ can diffuse out from the film and,
701 consequently, able to react with substrates present in solution we carried out steady-state
702 photolysis experiments in the presence of S^4TdR (4-Thiotymidine) and SOSG (Singlet Oxygen
703 Sensor Green) as suitable primary $^1O_2$ acceptors (Rizzi et al., 2014; Cellamare et al, 2013; Rizzi
704 et al., 2015; Ragas, Jimenez-Banzo, Sanchez-Garcia, Batllori & Nonell, 2009).
705 Figure 9a,b show results obtained upon irradiation of the film in the presence of SOSG and
706 S^4TdR, respectively. The irradiation of the CH/CD/Chl*a* film immersed in a D_2O solution
707 containing 10^{-5}M of S^4TdR, leads to the degradation of the latter (Figure 9b), as evidenced by the
708 bleaching of the main S^4TdR absorption band. Additionally, a red shift of the S^4TdR main
709 absorption band from 326 nm to 337 nm was observed. This result is not surprising since it
710 depends on the slight and slow releasing of H^+ from chitosan film, in such condition. In fact the
711 absorption of S^4TdR at neutral and acid pH is settled at around 337 nm (Rizzi et al., 2014;
712 Montalti, Credi, Prodi & Gandolfi, 2006) as it is clear from UV-Vis absorption spectrum in H_2O
713 (dashed line in Figure 9b). In the inset of the same Figure, measurement of control in absence of
714 Chl*a* is reported. In absence of photosensitizer, a clear red shifts of S^4TdR absorption peak is
715 showed after light irradiation, while it is not evidenced any absorbance decrease. Moreover as
716 indicated in the Figure 9b, a new band was detected at 270 nm when Chl*a* was presented in the
717 composite film, indicating the conversion of S^4TdR in Thymidine as the main $^1O_2$-induced
718 product (Rizzi et al, 2014). Results obtained in the presence of SOSG (Figure9a), a selective $^1O_2$

719 probe, confirmed the previous consideration indicating the photoactivity of Chitosan/Chl*a* film
720 under our experimental conditions.
721 In Figure 9a are reported photolysis experiments performed both in aqueous solution and in
722 D_2O medium, containing SOSG with CH/CD film and CH/CD/Chl*a* film in presence and in
723 absence of NaN_3 (10 mM), a well-known $^1O_2$ quencher (Cellamare et al., 2013). Looking at
724 Figure 9a, a fluorescence intensity decrease was observed in the first time of reaction in all
725 reported traces, with a subsequent fluorescence increase increasing the irradiation time.
726 However, in D_2O medium, the initial fluorescence decrease appears reduced. As reported in a
727 previous study performed by some of Authors of this paper (Cellamare et al., 2013), related to
728 Chl*a* in water solutions, the initial fluorescence decrease is similar to the results obtained for
729 SOSG without PS and irradiated in visible region. In fact, a fast intramolecular electron transfer
730 from anthracene moiety to fluorescein moiety occurs quenching the SOSG fluorescence
731 (Wilkinson, Helman & Ross, 1993; Ragas et al., 2009). Interestingly, this intramolecular electron
732 transfer reaction competes efficiently with SOSG fluorescence if the anthracene moiety is not
733 destroyed by singlet oxygen. As a consequence, when $^1O_2$ oxides the anthracene moiety to the
734 endoperoxide product, the intra-electron transfer reaction does not occurs and the SOSG
735 fluorescence increases. Not surprisingly, in the D_2O medium, where the $^1O_2$ lifetime occurs to be
736 greater than the one observed in water solutions (Xua et al.,2005), a higher amount of anthracene
737 moiety is oxidized by $^1O_2$ and subtracted from the intramolecular electron transfer reaction
738 increasing the fluorescence intensity in the first part of reaction. Moreover, the comparison of the
739 maximum fluorescence intensity values (see Figure 9a), obtained in the different conditions,
740 provides further information about the production of $^1O_2$ by chitosan film containing Chl*a*. In
741 fact experiments in presence of NaN_3 confirm clearly the proposed hypothesis. A significant

742 decrease of fluorescence intensity is observed comparing the I_{max} values recorded for
743 CH/CD/Chl*a* film in either H_2O or D_2O without NaN_3. On the other hand, as shown in Figure 9c,
744 there is a progressive bleaching of Chl*a* absorbance with elapsing the irradiation time. In 10
745 minutes, the absorbance of main absorption bands in the red and blue regions decreases of about
746 15%. After a prolonged time of irradiation, the absorption intensity at 661 nm decreased of about
747 50% in 100 minutes, while an increase in absorbance intensity at wavelengths above 690 nm and
748 between 460 and 580 nm was also observed. These results are in good agreement with those
749 reported in literature (Barazzouk et al., 2012b). Barazzouk and co-workers (2012b) display
750 studies in which the photodegradation of Chl*a* in several conditions was well described,
751 ascribing such behavior to the production of ROS. Clearly the observed photobleaching of the
752 pigment, under this condition, suggests that Chl*a* itself appears as an indirect molecular probe for
753 toxic species, decreasing its absorption intensity during light irradiation.
754 The overall results indicate the involvement of $^1O_2$ and probably of other ROS. Procedures
755 addressed to improve the photostabilty of Chl*a* preventing the ROS-attack will be developed, in
756 the next future in our laboratories.
757
758 **4. Conclusions**
759 In the present paper, different Chitosan and Chitosan/2-HP-β-CD composite films have been
760 obtained and the latter has been successfully modified by inserting Chl*a* casted by an ethanolic
761 solution. An innovative procedure, recently developed in our laboratory has been employed to
762 reduce the intrinsic acidity of chitosan film in order to introduce Chl*a* maintaining its physical
763 and chemical properties. Each polysaccharide component of the composite films plays a specific
764 role in the interactions with chitosan water-retained, and 2-HP-β-CD increasing the hydrophobic

properties of the films. DSC and WVTR analyses show the increased hydrophobic character of the Chitosan films in the presence of 2-HP-β-CD and Chl*a* offering good perspective for extending shelf-life or improve safety properties maintaining the quality of the food. Our comprehensive investigation demonstrates that Chl*a* molecules have a strong affinity towards the Chitosan/2-HP-β-CD mixture and spectroscopic analyses indicate that Chl*a* interacts with amino groups of chitosan chains. The morphological investigations carried out by SEM and AFM images, demonstrate that Chl*a* is uniformly distributed on Chitosan film. In addition the contact with EtOH induces a novel chitosan chain interactions rendering the chitosan film structure much more compact than previous the treatment. XRD analysis shows the existence of an amorphous phase for all the investigated samples. Additionally the photodynamic effects of Chl*a* has been also investigated. Nanosecond laser flash photolysis technique provides clear evidence for the population of the excited triplet state of Chl*a* and the photogeneration of singlet oxygen is demonstrated by both direct detection by using infrared luminescence spectroscopy and chemical methods based on the use of suitable traps.

ASSOCIATED CONTENT

Supporting Information. Chl*a* extraction procedure, WVTR film data, a table with XPS surface atomic concentrations, the SEM images of different chitosan films, the AFM Phase images of "as prepared" and upon treatment related to CH and CH/CD films, the XRD patterns of the different chitosan films.

AUTHOR INFORMATION

Corresponding Author

*Prof. Pinalysa COSMA

Università degli Studi di Bari "Aldo Moro"

Dipartimento di Chimica

Via Orabona, 4

I-70126 Bari, ITALY

e-mail: pinalysa.cosma@uniba.it

tel. +39 0805443443

fax +39 0805442128.

ACKNOWLEDGMENT

This study was supported by the PRIN-MIUR 2010-2011 (Prot. 2010C4R8M8) funding program: "Architetture ibride multifunzionali basate su biomolecole per applicazioni nel campo della sensoristica, della conversione di energia e del biomedicale". We gratefully acknowledge the skilfull and excellent technical assistance of Mr. Sergio Nuzzo and Mr. Savino Cosmai and Dr. Andrea Ventrella for the excellent and precious collaboration in the determination of the chitosan acetylation degree.

REFERENCES

Agostiano, A., Catucci, L., Castagnolo, M., Colangelo, D., Cosma, P., Fini, P., & Della Monica, M. (2002a). Interaction between chlorophyll a and beta-cyclodextrin derivatives in aqueous solutions - Spectroscopic and calorimetric study. *J. Therm. Anal. Calorim.*, *70*, 115-122.

Agostiano, A., Catucci, L., Colafemmina, G., & Della Monica, M. (1996). Chlorophyll a self-organization in microheterogeneous surfactant systems. *Biophys. Chem., 60(1-2)*, 17-27.

Agostiano, A., Catucci, L., Colafemmina, G.,&Scheer, H. (2002b). Role of functional groups and surfactant charge in regulating chlorophyll aggregation in micellar solutions. *J. Phys. Chem.*B, *106*, 1446-1454.

Agostiano, A., Catucci, L., Cosma, P., & Fini, P. (2003). Aggregation processes and photophysical properties of chlorophyll a in aqueous solutions modulated by the presence of cyclodextrins. *Phys. Chem. Chem. Phys.*, *5*, 2122-2128.

Agostiano, A., Cosma, P., Trotta, M., Monsù-Scolaro, L., & Micali, N. (2002). Chlorophyll a behavior in aqueous solvents: Formation of nanoscale self-assembled complexes. *J. PhysicalChem. B*, *106(49)*, 12820-12829.

Agostiano, A., Cosma, P., & Della Monica, M. (1991). Formation of chlorophyll-a photoreactive dimers in alcoholic mixtures - spectroscopic and electrochemical study. *J. Photochem. Photobiol. A: Chemistry*, *58(2)*, 201-213.

Agostiano, A., Cosma, P., Della Monica, M.,&Fong, F. K. (1990). Spectroscopic and electrochemical characterization of chlorophyll-a in different water + organic-solvent mixtures. *Bioelectroch. Bioenerg. 23(3)*, 311-324.

B. H. Stuart. *Infrared Spectroscopy: Fundamentals and Applications*. (2004). In Wiley, Analytical Technique in the Sciences.

Baxter, A., Dillon, M., Taylor, K.D., & Roberts, G.A.F. (1992). Improved method for IR determination of the degree of N-acetylation of chitosan. *Int J Biol. Macromol.*, *14*, 166–169.

Beamson G., & Briggs D. (1992). High Resolution XPS of Organic Polymers, J. Wiley & Sons, Chichester.

Bekalé, L., Barazzouk, S., & Hotchandani, S. (2012a). Beneficial role of gold nanoparticles as photoprotector of magnesium tetraphenylporphyrin. *J. Mater. Chem.*, *22*, 2943-2951.

Bekalé, L., Barazzouk, S., & Hotchandani, S. (2012b). Enhanced photostability of chlorophyll-a using gold nanoparticles as an efficient photoprotector. *J. Mater. Chem*., *22*, 25316-25324.

Belalia, R., Grelier, S., Benaissa, M., & Coma, V. (2008). New bioactive biomaterials based on quaternized chitosan. *J. Agric. Food Chem*., *56*, 1582-1588.

Bordenave, N., Grelier, S., & Coma, V. (2010). Hydrophobization and Antimicrobial Activity of Chitosan and Paper-Based Packaging Material. *Biomacromol*. *11,* 88-96.

Bordenave, N., Grelier, S., Pichavant, F., & Coma, V. (2005). Water and moisture susceptibility of chitosan and paper-based materials: Structure-property relationships. *J. Agr. Food Chem*., *55*, 9479-9488.

Bostan, M.S., Mutlu, E.C., Kazak, H., Keskin, S.S., Oner, E.T., & Eroglu, M.S. (2014). Comprehensive characterization of chitosan/PEO/levan ternary blend films. *Carbohydrate Polymers.*, *102*, 993-1000.

Brace, J. G., Fong, F. K., Karweik, D. H., Koester, V. J., Shepard, A. & Winograd, N. (1978). Stoichiometric determination of chlorophyll a-water aggregates and photosynthesis. Symbiotic roles of the magnesium atom and the ring V cyclopentanone group in the structural and photochemical properties of chlorophyll a monohydrate and dehydrate. *J. Am. Chem. Soc.*, *100*, 5203-2507.

851 Burns, N.A., Burroughs, M.C., Gracz, H, Pritchard, C.Q., Brozena, A.H., Willoughby, J., &
852 Khan, S.A. (2015). Cyclodextrin facilitated electrospun chitosan nanofibers. *RSCAdv*., *5*, 7131-
853 7137.

854 Cellamare, B.M., Fini, P., Agostiano, A., Sortino, S. & Cosma, P. (2013). Identification of ROS
855 Produced by Photodynamic Activity of Chlorophyll/Cyclodextrin Inclusion Complexes.
856 *Photochem. Photobiol.*, *89*, 432-441.

857 Cerveny, K.E., De Paola, A., Duckworth, S.H., & Gulig, P.A. (2002). Phage therapy of local and
858 systemic disease caused by Vibrio vulnificus in iron-dextran-treated mice. *Infection and*
859 *Immunity*, *70*, 6251-6262.

860 Chauvet, J. P., Viovy, R., Santus, R., & Land, E.J. One-electron oxidation of photosynthetic
861 pigments in micelles. Bacteriochlorophyll a, chlorophyll a, chlorophyll b, and pheophytin a. *J.*
862 *Phys. Chem*., *85(23)*, 3449-3456.

863 Chen, G., Mi, J., Wu, X., Luo, C.L., Li, J.B., Tanng, Y.X., & Li, J. (2011). Structural features
864 and bioactivities of the chitosan. *Int. J.Biol. Macromol*., *49,* 543-547.

865 Chen, P.H., Kuo, T.Y., Liu, F. H., Hwang, Y.H., Ho, M.H., Wang, D.M., Lai, J.Y., & Hsieh, H.J.
866 (2008). Use of dicarboxylic acids to improve and diversify the material properties of porous
867 chitosan membranes. *J.Agric. Food Chem.*, *56*, 9015-9021.

868 Chiono, V., Gentile, P., Boccafoschi, F., Carmagnola, I., Ninov, M., Georgieva, V., Georgiev,
869 G., & Ciardelli, G. (2010). Photoactive Chitosan Switching on Bone-Like Apatite Deposition.
870 *Biomacromol*., *11*, 309-315.

871 Coma, V. (2013). Polysaccharide-based Biomaterials with Antimicrobial and Antioxidant
872 Properties. *Polímeros.*, *23(3),* 287-297.

873 Davies, D.H., Elson, C.M., & Hayes, E.R. (1989). Chitin and chitosan: sources, chemistry,
874 biochemistry, physical properties and applications. In G. Skjak-Braek, T. Anthonsen, P. &
875 Sandford P. (Eds) (pp. 467-72). England: Elsevier Appl. Sci.

876 Demarger-Andre, S.,& Domard, A. (1994). Chitosan carboxylic acid salts in solution and in the
877 solid state. *Carbohydrate Polymers*, *23*, 211-219.

878 Dentuto, P.L., Catucci, L., Cosma, P., Fini, P., Agostiano, A., Hackbarth, S., Rancan, F., &
879 Roeder, B. (2007). Cyclodextrin/chlorophyll a complexes as supramolecular photosensitizers.
880 *Bioelectrochem., 70*, 39-43.

881 El Ghaouth, A., Arul, J., Grenier, J., & Asselin, A. (1992). Antifungal activity of chitosan on 2
882 postharvest pathogens of strawberry fruits. *Phytopathol.*, *82*, 398-402.

883 El Ghaouth, A., Arul, J., Ponnampalam, R., & Boulet, M. (1991). Chitosan coating effect on
884 storability and quality of fresh strawberries. *J. Food Sci.*, *56*, 1618-1620.

885 El-Hefian, E.A., Nasef, M.M., & Yahaya, A.H. (2012). Preparation and Characterization of
886 Chitosan/Agar Blended Films: Part 1. Chemical Structure and Morphology. *E-Journal of*
887 *Chemistry*, *9(3)*, 1431-1439.

888 Fu, D., Jordan, J.J., & Samson, L.D. (2013). Human ALKBH7 is required for alkylation and
889 oxidation-induced programmed necrosis. *Genes Dev*, *27*, 1089-1100.

Gomez-Estaca, J., Lopez-de-Dicastillo, C., Hernandez-Munoz, P., Catala, R., & Gavara, R. (2014). Advances in antioxidant active food packaging. *Trends in Food Science & Technology*. *35*, 42-51

Hamblin, M.R., & Hasan, T. (2004) Photodynamic therapy: a new antimicrobial approach to infectious disease? *Photochem. Photobiol. Sci.*, *3(5)*, 436-450.

Harish Prashanth, K.V., Kittur, F.S., & Tharanathan, R.N. (2002). Solid state structure of chitosan prepared under different N-deacetylating conditions. *Carbohydrate Polymers*, *50(1)*, 27-33.

He, Q., Ao, Q., Gong, Y., & Zhang, X. (2011). Preparation of chitosan films using different neutralizing solutions to improve endothelial cell compatibility. *J. Mater Sci: Mater. Med.* 22, 2791-2802.

J. Coates. (2000). *Interpretation of Infrared Spectra, A Practical Approach.* In John Wiley & Sons Ltd. Encyclopedia of Analytical Chem (Eds: R.A. Meyers). (pp. 10815–10837). Chichester.

Jiang, Y., & Li, Y. (2001). Effects of chitosan coating on postharvest life and quality of longan fruit. *Food Chem.73*, 139-143.

Jug, M., Maestrelli, F., & Mura, P. (2012). Native and polymeric β-cyclodextrins in performance improvement of chitosan films aimed for buccal delivery of poorly soluble drugs. *J. Incl. Phenom. Macrocycl. Chem.*, *74*, 87-97.

Kang, J., Liu, H., Zheng, Y.-M., Qu, J., & Chen, J. (2010). P.Systematic study of synergistic and antagonistic effects on adsorption of tetracycline and copper onto a chitosan. *J. Colloid Interface Sci*., *344*, 117-125.

911 Karweik, D. H., & Winograd, N. (1976). Nitrogen charge distributions in free-base porphyrins,
912 metalloporphyrins, and their reduced analogs observed by x-ray photoelectron spectroscopy.
913 *Inorg. Chem.*, *15*, 2336-2342.

914 Kasaai, R. (2008). A review of several reported procedures to determine the degree of N-
915 acetylation for chitin and chitosan using infrared spectroscopy. *Carbohydrate Polym.*, *71*,
916 497-508.

917 Kittur, F.S., Harish Prashanth, K.V., Sankar, K.U., & Tharanathan, R.N. (2002). Characterization
918 of chitin, chitosan and their carboxymethyl derivatives by differential scanning calorimetry.
919 *Carbohydrate polymers. 49 (2)*, 185-193.

920 Krajewska, B. (1991). Chitin and its derivatives as supports for immobilization of enzymes. *Acta*
921 *Biotechnol. 11*, 269-277.

922 Krajewska, B., Leszko, M., & Zaborska, W. (1990) Urease immobilized on chitosan membrane -
923 preparation and properties. *J. Chem. Technol. Biotechnol*., *48*, 337-350.

924 Krouit, M., Granet, R., Branland, P., Verneuil, B. & Krausz, P. (2006). New photoantimicrobial
925 films composed of porphyrinated lipophilic cellulose esters. *Bioorganic & Medicinal Chemistry*
926 *Letters, 16(6)*, 1651–1655.

927 Krouit, M., Granet, R. & Krausz, P. (2009). Photobactericidal films from porphyrins grafted to
928 alkylated cellulose – synthesis and bactericidal properties. *European Polymer Journal, 45(4),*
929 1250–1259.

930 Lavertu, M., Xia, Z., Serreqi, A.N., Berrada, M., Rodrigues A., Wang, D., Buschmann
931 M.D., & Gupta, A. A. (2003). Validated 1H NMR method for the determination of then
932 degree of deacetylation of chitosan. *J Pharmaceut Biomed*., *32*, 1149-1158.
933 Liu, H., Adhikari, R., Guo, Q., & Adhikari, B. (2013). Preparation and characterization of
934 glycerol plasticized (high-amylose) starch–chitosan films. *J Food Eng*. *116*, 588-597.

935 Mandal, P., Manna, J.S., Das, D., & Mitra, M.K. (2015). Excitonic dynamics of Chlorophyll-a
936 molecules in chitosan hydrogel scaffold. *J. Photochem. Photobiol Sci., 14*, 786-791.

937 Manna, J.S.,Basu, S.,Mitra, M.K. Mukherjee, S., & Das, G.C. (2009). Study on the biostability
938 of chlorophyll a entrapped in silica gel nanomatrix. *J. Mater Sci:Mater Electron*, *20*, 1068-1072.

939 Mbakidi, J.P., Herke, K., Alvès, S., Chaleix, V., Granet, R., Krausz, P., Leroy-Lhez, S., Ouk,
940 T.S. & Sol, V. (2013). Synthesis and photobiocidal properties of cationic porphyrin-grafted
941 paper. *Carbohydrate Polymers*, *91(1,2)*, 333–338

942 Moczek, L., & Nowakowska, M. (2007) Novel water-soluble photosensitizers from chitosan.
943 *Biomacromol.*, *8*, 433-438.

944 Muzzarelli, R.A.A., &Rocchetti, R. (1986) *Chitin in Nature and Technology*. In R.A.A.
945 Muzzarelli, C. Jeuniaux & G.W. Gooday (Eds) (pp. 385-388). New York: Plenum Press.

946 Nunthanid, J., Puttipipatkhachorn, S., Yamamoto, K., & Peck, G.E. (2001). Physical Properties
947 and Molecular Behavior of Chitosan Films. *Drug Dev. Ind. Pharm., 27(2),* 143-157.

948 Ogawa, K., Hirano, S., Miyanishi, T., Yui, T., & Watanabe, T. (1984). A new polymorph of
949 chitosan. *Macromolecules*, *17*, 973-975.

950 Omata, T., & Murata, N.A. (1980). A rapid and efficient method to prepare chlorophyll a and b
951 from leaves. *Photochem. Photobiol.*, *31*, 183-185.

952 Osman, Z., & Arof, A.K. (2003). FTIR studies of chitosan acetate based polymer electrolytes.
953 *Electrochimica Acta. 48*, 993-999.

954 Pedersen, M. F., Stæhr, P.A., Wernberg, T., & Thomsen, M.S. (2005). Biomass dynamics of
955 exotic Sargassum muticum and native Halidrys siliquosa in Limfjorden, Denmark - Implications
956 of species replacements on turnover rates. *Aquatic Botany*. *83*, 31-47.

957 Pereira Jr., V.A., Queiroz de Arruda, I.N., & Stefani, R. (2015). Active chitosan/PVA films with
958 anthocyanins from Brassica oleraceae (Red Cabbage) as Time–Temperature Indicators for
959 application in intelligent food packaging. *Food Hydrocolloid*. *43(1)*, 180-188.

960 Philippova, O. E., Volkov, E.V., Sitnikova, N. L., & Khokhlov, A. R. (2001). Two Types of
961 Hydrophobic Aggregates in Aqueous Solutions of Chitosan and Its Hydrophobic Derivative.
962 *Biomacromol*., *2*, 483-490.

963 Quintavalla, S., & Vicini, L. (2002). Antimicrobial food packaging in meat industry. *Meat*
964 *Science industry*., *62(3)*, 373-380.

965 Rabea, E.I., Badawy, M.E.T., Stevens, C.V., Smagghe, G., & Steurbaut, W. (2003) Chitosan as
966 antimicrobial agent: Applications and mode of action. *Biomacromol.*, *4*, 1457-1465.

967 Ringot, C., Sol, V., Barrière, M., Saad, N., Bressollier, P., Granet, R., Couleaud, P., Frochot, C.
968 & Krausz, P. (2011). Triazinyl Porphyrin-Based Photoactive Cotton Fabrics: Preparation,
969 Characterization, and Antibacterial Activity, *Biomacromolecules*, *12(5),* 1716–1723

970 Rizzi, V., Longo, A., Fini, P., Semeraro, P., Cosma, P., Franco, E., García, R., Ferrándiz, M.,
971 Núñez, E., Gabaldón, J.A., Fortea, I., Pérez, E., &Ferrándiz, M. (2014). Applicative Study (Part
972 I): The Excellent Conditions to Remove in Batch Direct Textile Dyes (Direct Red, Direct Blue
973 and Direct Yellow) from Aqueous Solutions by Adsorption Processes on Low-Cost Chitosan
974 Films under Different Conditions. *Advances in Chemical Engineering and Science*, *4*, 454-469.

975 Rizzi, V., Losito, I., Ventrella, A., Fini, P., Agostiano, A., Longobardi, F., & Cosma, P. (2014).
976 pH-related features and photostability of 4-thiothymidine in aqueous solution: an investigation
977 by UV-visible, NMR and FTIR-ATR spectroscopies and by electrospray ionization mass
978 spectrometry. *RSC Adv. 4*, 48804-48814.

979 Rizzi, V., Losito, I., Ventrella, A., Fini, P., Fraix, A., Sortino, S., Agostiano, A., Longobardi,
980 F. & Cosma, P. (2015). Rose Bengal-photosensitized oxidation of 4-thiothymidine in aqueous
981 medium: evidence for the reaction of the nucleoside with singlet state Oxygen.
982 *Phys.Chem.Chem.Phys*., *17*, 26307

983 Roy, P. S., Samanta, A., Mukherjee, M., Roy, B. & Mukherjee, A. (2013). Designing Novel pH-
984 Induced Chitosan–Gum Odina Complex Coacervates for Colon Targeting. *Ind. Eng. Chem. Res*.,
985 *52*, 15728-15745.

986 Ryan, A. A., & Senge, M.O. (2015). How green is green chemistry? Chlorophylls as a
987 bioresource from biorefineries and their commercial potential in medicine and photovoltaics.
988 *Photochem. Photobiol. Sci*., *14*, 638-660.

989 Sajjan, U.S., Tran, L.T., Sole, N., Rovaldi, C., Akiyama, A., Friden, P.M., Forstner, J.F., &
990 Rosthstein, D.M. (2001). P-113D, an antimicrobial peptide active against Pseudomonas

aeruginosa, retains activity in the presence of sputum from cystic fibrosis patients. *Antimicrob. Agents Chemother*, *45*, 3437-3444.

Shrestha, A., & Kishen, A. (2012). Polycationic Chitosan-Conjugated Photosensitizer for Antibacterial Photodynamic Therapy. *Photochem. Photobiol*., *88*, 577-583.

Synytsya, A., Grafová, M., Slepicka, P., Gedeon, O., & Synytsya, A. (2012). Modification of Chitosan–Methylcellulose Composite Films with meso-Tetrakis(4-sulfonatophenyl)porphyrin. *Biomacromol.*, *13(2)*, 489-498.

Thakhienw, W., Devahastin, S., & Soponronnarit, S. (2013). Physical and mechanical properties of chitosan films as affected by drying methods and addition of antimicrobial agent. *J Food Eng*. *119*, 140-149.

Vermeiren, L., Devlieghere, F., Van Beest, M., De Kruijf, N., & Debevere, J. (1999). Developments in the active packaging of foods. *Trends in Food Science & Technology*, *10*, 77-86.

Wainwright, M. (1998). Photodynamic antimicrobial chemotherapy (PACT). *J. Antimicrob. Chemother. 42(1)*, 13-28.

Wang, H.D., Chu, L.Y., Song, H., Yang, J.P., Xie, R., & Yang, M. (2007). Preparation and enantiomer separation characteristics of chitosan/β-cyclodextrin composite membranes. *Membrane Sci.*, *297*, 262-270.

Xu, Y.X., Kim, K.M., Hanna, M.A., & Nag, D. (2015). Chitosan–starch composite film: preparation and characterization. *Ind. Crop Prod.*, *21*, 185-192.

1011 Yoshikawa, T. T. (2002) Antimicrobial Resistance and Aging. *J Am Geriatr. Soc*., *50*, S226-
1012 S229.

Figure Captions

Figure 1: UV-Visible Absorption spectra of **(a)** CH/CD film containing Chl*a* and **(b)** Ethanolic solution of Chl*a* at concentration of 10^{-5}M. *Inset 1a*: First derivative analysis of UV-Vis absorption spectrum of CH/CD film containing Chl*a*. The camera picture of a large sample CH/CD/Chl*a* showing the homogeneous distribution of Chl*a* inside the film.

Figure 2: High-resolution XPS C 1s and N 1s spectra of **(a)** the CH film prepared with the new method (CH) after immersion in ethanol, **(b)** the CH/CD film after immersion in ethanol and **(c)** the CH/CD/Chl*a* film

Figure 3 Comparison between detailed views (Temperature range: 0-300°C) of DSC thermograms of **(a)** Chl*a* samples prepared by casting from ethanol solution in the aluminum

Figure 4: Comparison between detailed views (wavenumber range: 600-4000 cm-1) of ATR-FTIR spectra of different composite films: (a) Chitosan films (CH) containing 2-HP-β-CD in presence (gray line) and in absence (black line) of Chl*a*; (b) Chitosan films containing 2HP-β-CD (CH/CD) before (black line) and after treatment with EtOH (gray line); (c) Chitosan films in presence (gray line, CH/CD) and in absence (black line, CH) of cyclodextrin; (d) Chitosan films obtained in accordance with standard procedure (black line CH STD) and chitosan film in accordance with our method (gray line, CH).

Figure 5: AFM images of "as prepared" **(a-c)** and upon treatment with EtOH **(d-f)** related to CH STD, CH, and CH/CD films, respectively

Figure 6: AFM **(a)** topography and **(b)** phase of CH/CD/Chl *a* film

Figure 7. Transient absorption spectrum observed 0.2 μs after 355 laser excitation of the CH/CD/Chl*a* film. $E_{355} \approx 10$ mJ/pulse. The inset shows the decay profile monitored at 460 nm.

Figure 8. Singlet oxygen luminescence observed upon 405 nm CW laser excitation (2 W cm^{-2}) of a CH/CD/Chl*a* film immersed in D_2O.

Figure 9: **(a)**Time evolution of normalized fluorescence emission at 525 nm of SOSG 1.5 μM of aqueous solutions containing CH/CD/Chl*a* film in different conditions. (see text for details) **(b)** Time evolution of S^4TdR absorption (10^{-5}M) spectrum of aqueous solutions containing CH/CD/Chl*a* film. Dotted line was

referred to an aqueous solution, pH 6.5, in absence of CH containing only S^4TdR (see text for details) **(c)** Time evolution of absorption CH/CD/Chl*a* spectrum (see text for details) under visible.

Figure

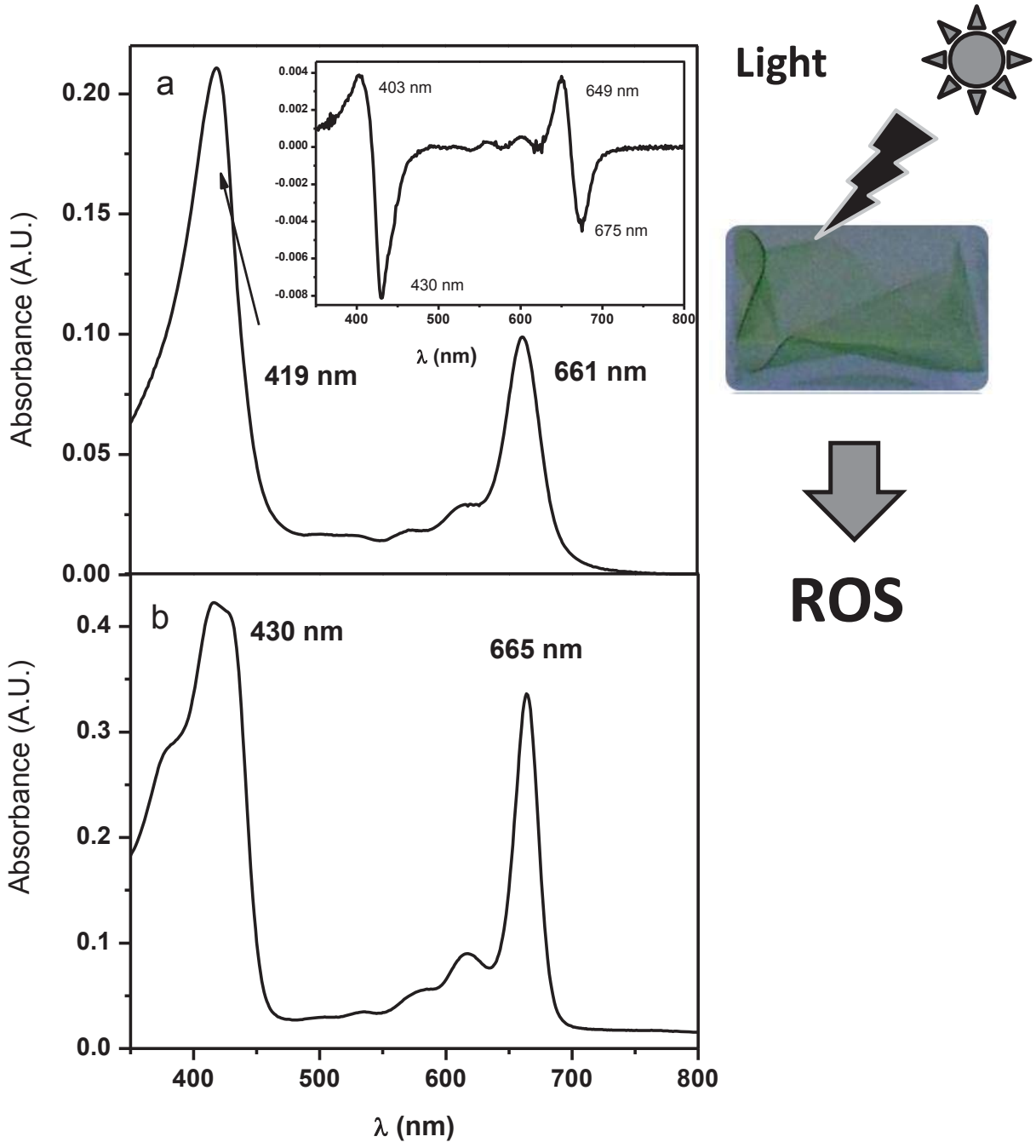

Figure 1

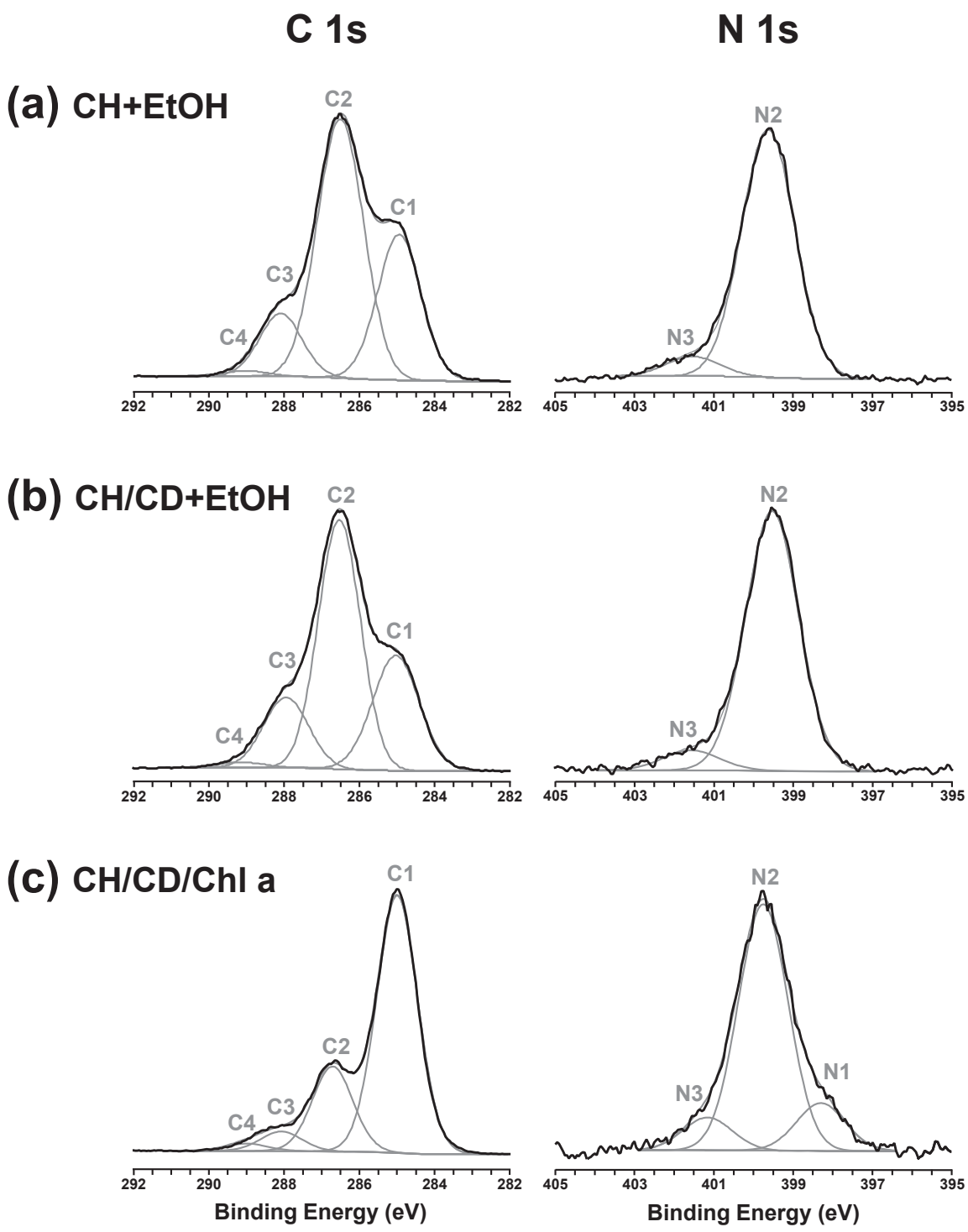
C 1s
N 1s
(a) CH+EtOH
C2
C1
C3
C4
N2
N3
292
290
288
286
284
282
405
403
401
399
397
395
(b) CH/CD+EtOH
C2
C1
C3
C4
N2
N3
(c) CH/CD/Chl a
C1
C2
C3
C4
N2
N1
N3
Binding Energy (eV)
Binding Energy (eV)

Figure 2

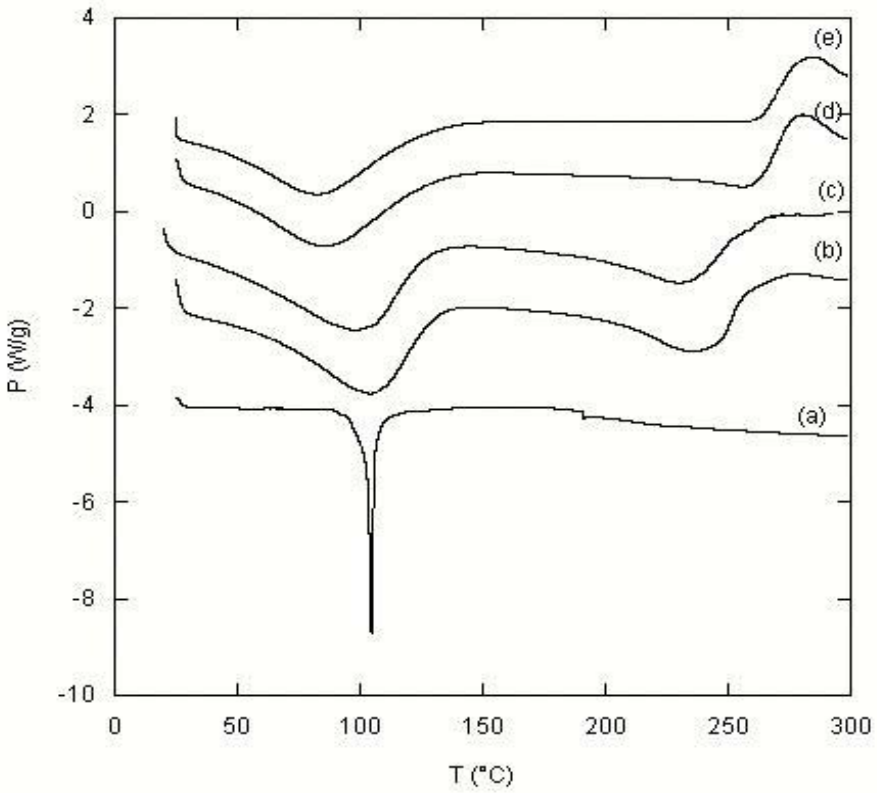

Figure 3

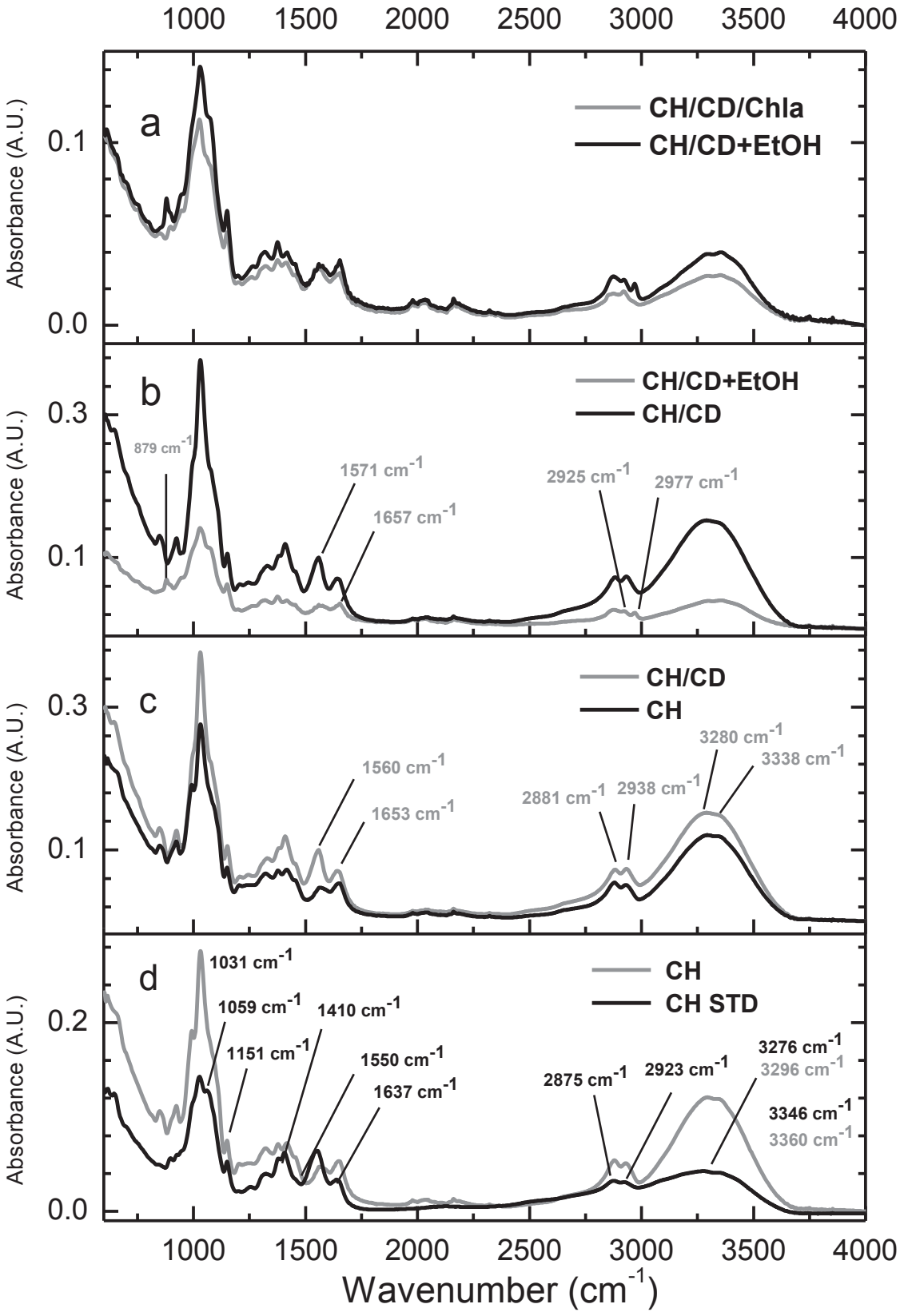
a
CH/CD/Chla
CH/CD+EtOH
b
CH/CD+EtOH
CH/CD
879 cm-1
1571 cm-1
1657 cm-1
2925 cm-1
2977 cm-1
c
CH/CD
CH
1560 cm-1
1653 cm-1
2881 cm-1
2938 cm-1
3280 cm-1
3338 cm-1
d
CH
CH STD
1031 cm-1
1059 cm-1
1151 cm-1
1410 cm-1
1550 cm-1
1637 cm-1
2875 cm-1
2923 cm-1
3276 cm-1
3296 cm-1
3346 cm-1
3360 cm-1
Absorbance (A.U.)
Wavenumber (cm-1)

Figure 4

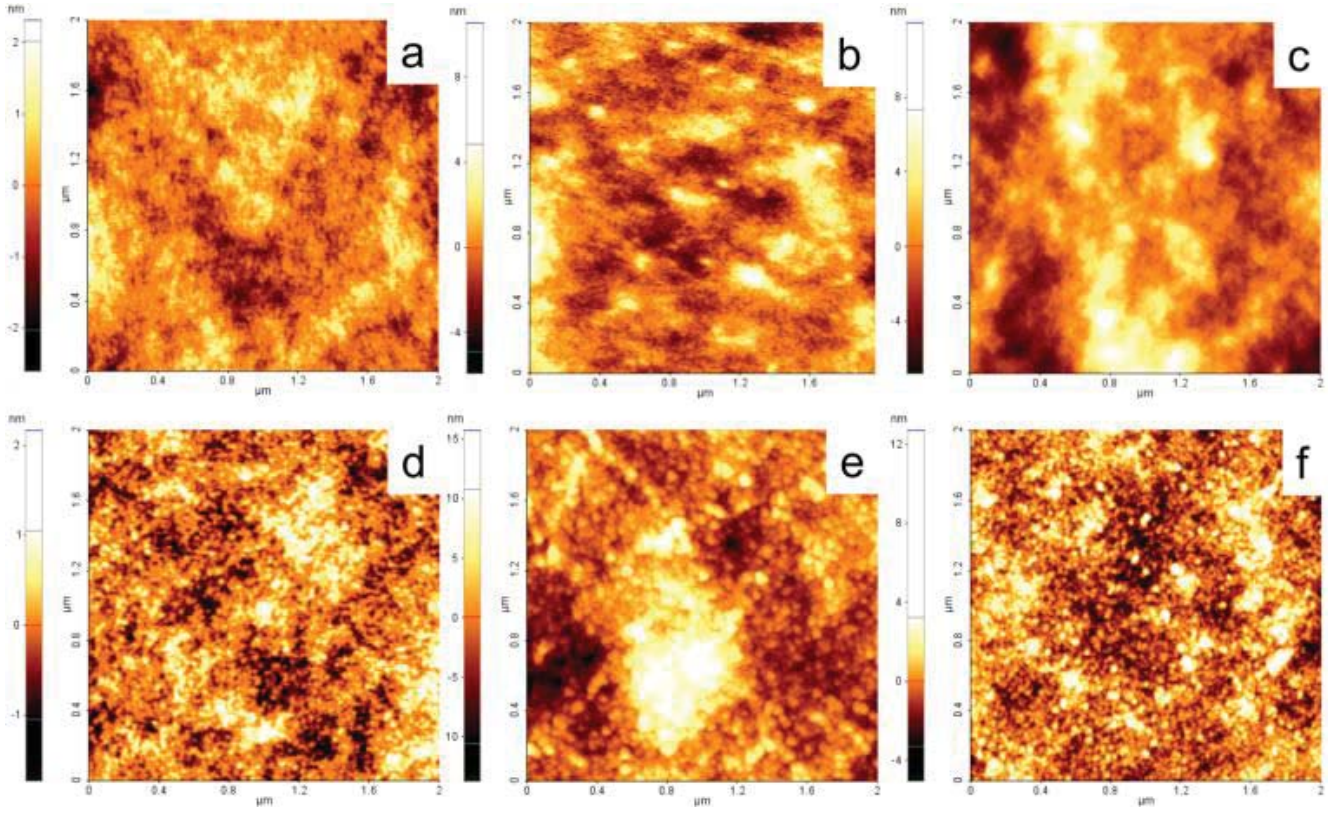

Figure 5

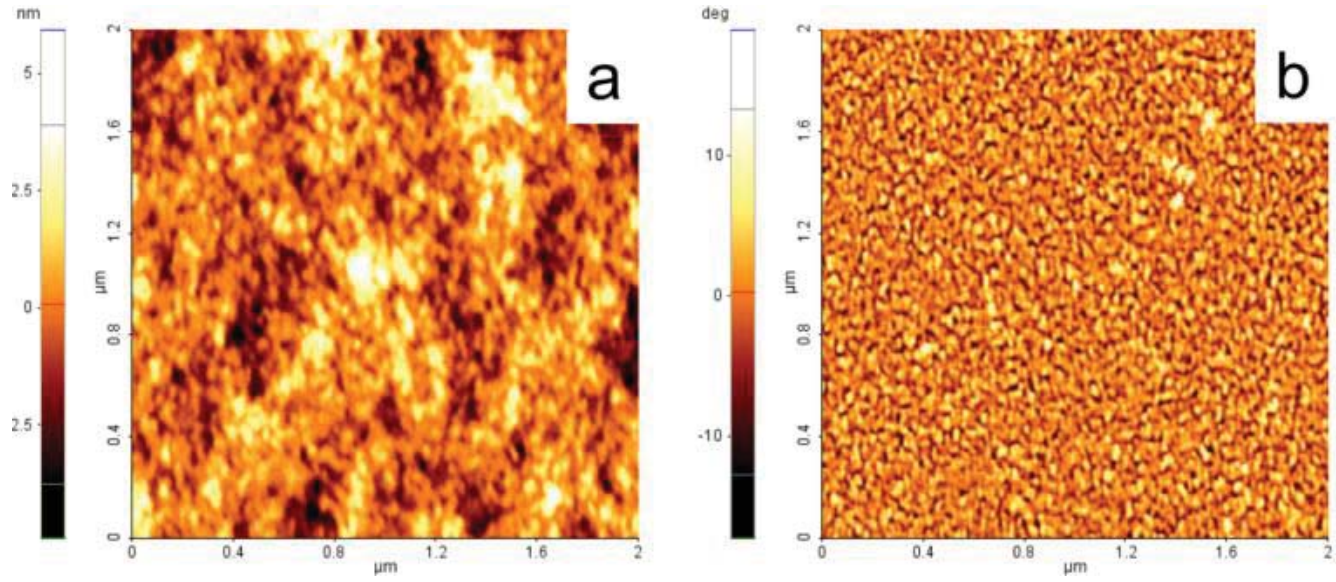

Figure 6

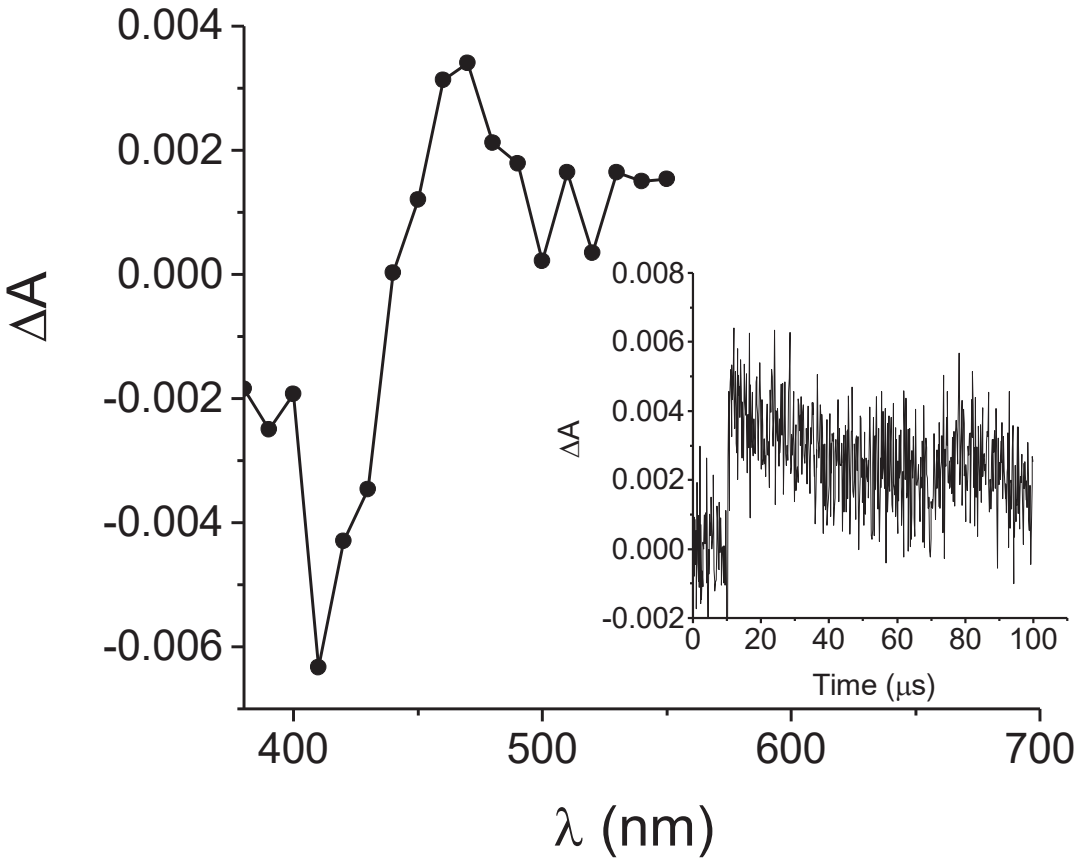
0.004
0.002
0.000
-0.002
-0.004
-0.006
ΔA
400
500
600
700
λ (nm)
0.008
0.006
0.004
0.002
0.000
-0.002
ΔA
0
20
40
60
80
100
Time (μs)

Figure 7

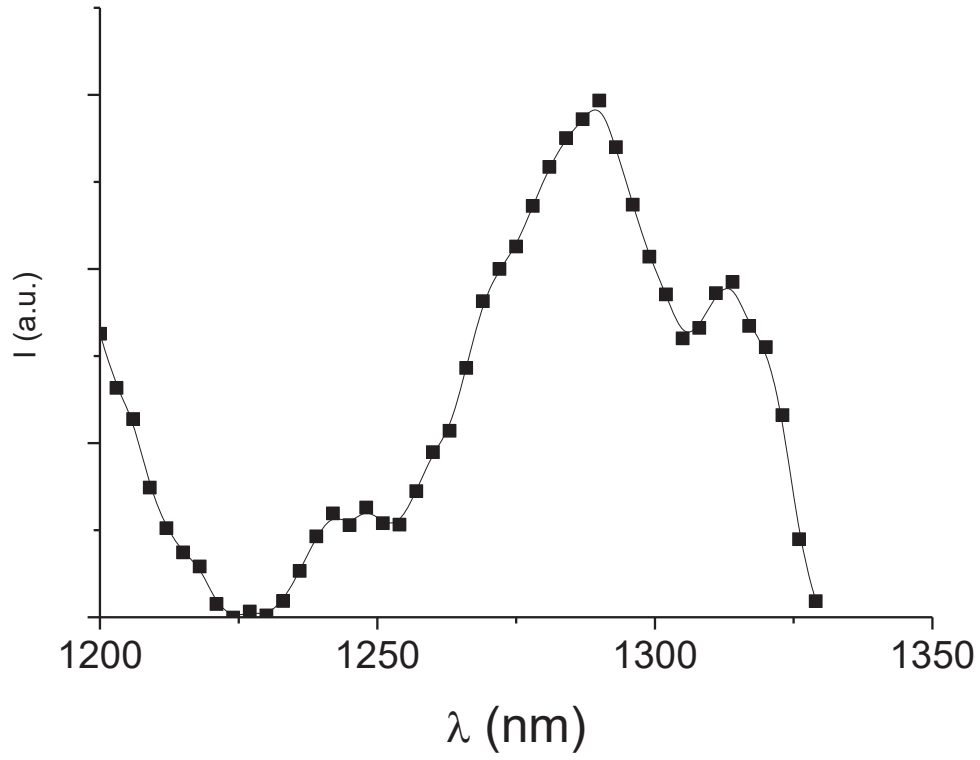

Figure 8

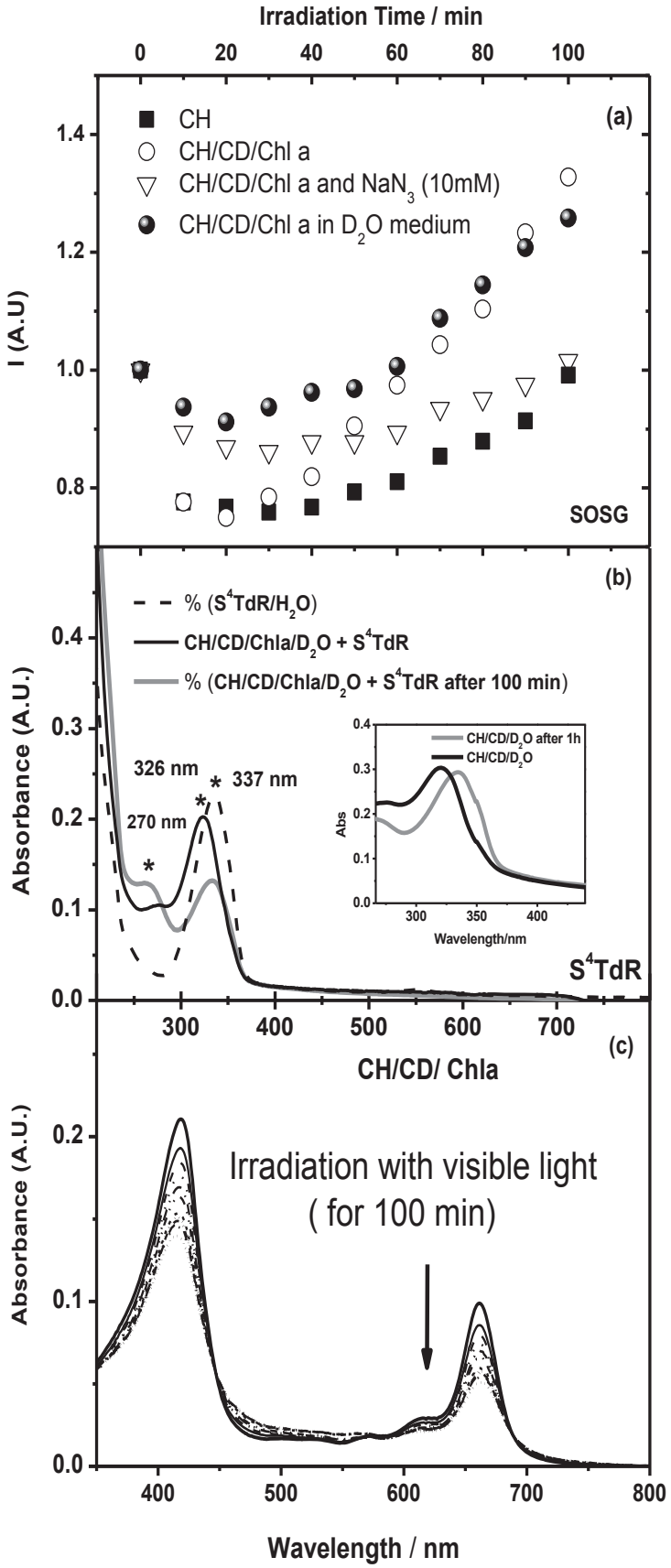
Irradiation Time / min
0
20
40
60
80
100
(a)
CH
CH/CD/Chl a
CH/CD/Chl a and NaN3 (10mM)
CH/CD/Chl a in D2O medium
I (A.U)
SOSG
(b)
% (S4TdR/H2O)
CH/CD/Chla/D2O + S4TdR
% (CH/CD/Chla/D2O + S4TdR after 100 min)
326 nm
337 nm
270 nm
CH/CD/D2O after 1h
CH/CD/D2O
Abs
Wavelength/nm
Absorbance (A.U.)
S4TdR
CH/CD/ Chla
(c)
Irradiation with visible light
(for 100 min)
Absorbance (A.U.)
Wavelength / nm

Figure 9

Table

Table 1. Curve-fitting results of the high-resolution XPS C 1s and N 1s spectra of **(a)** the CH film prepared with the new method after immersion in ethanol, **(b)** CH/CD film after immersion in ethanol and **(c)** CH/CD/Chl *a* film.

Signal	Component	Binding energy [eV]	Assignments	Relative peak area [%]		
				(a) CH + EtOH	(b) CH/CD + EtOH	(c) CH/CD/Chl *a*
C1s	C1	285.0	C-C, C-H, C=C	30	29	68
	C2	286.5	C-O, C-N	56	54	24
	C3	288.1	O–<u>C</u>–O, C=O,N–<u>C</u>=O	13	16	6
	C4	289.1	O-<u>C</u>=O	1	1	2
N 1s	N1	398.3	=N-			13
	N2	399.7	NH_2, <u>N</u>–C=O	93	93	78
	N3	401.5	NH_3^+	7	7	9

Supporting Information

Preparation, characterization and photoactivity of Chlorophyll a/Chitosan/2-HP-β-Cyclodextrin composite films: potential application for antimicrobial packaging.

Vito Rizzi[a], *Paola Fini*[b], *Fiorenza Fanelli*[c], *Tiziana Placido*[a], *Paola Semeraro*[a], *Teresa Sibillano*[d], *Aurore Fraix*[e], *Salvatore Sortino*[e], *Angela Agostiano*[a,b], *Cinzia Giannini*[d], *Pinalysa Cosma*[a,b]*

EXPERIMENTAL DETAILS

Chemicals. All the chemicals used were of analytical grade and samples were prepared using double-distilled water. Commercial grade Chitosan powder (CH, from crab shells, with a molecular weight of 150000, highly viscous, with a hypothetical deacetylation degree ≥ 75%), Acetic acid (99,9 %), EtOH (99,9 %) and glycerol (99,9 %) were purchased from Sigma Aldrich.

Not surprisingly, NMR and IR results were agreed between them, giving a DS(Ac) % around 30 % confirming the manufacturer's Sigma Aldrich specification. Chl*a* stock

solutions were stored in acetone at -80°C. 2-HP-β-CD was purchased from Fluka and used without further purification.

Chitosan deacetylation degree. Among several methods proposed for measuring the real degree of acetylation, DS(Ac), of CH, ^{1}H-NMR (700 MHz) and FTIR-ATR analyses have been used.

^{1}H-NMR measurements were performed by a Bruker AVANCE III 700 MHz spectrometer (Bruker BioSpin GmbH, Rheinstetten, Germany), equipped with a 5 mm 1H/D-BB probe head, with z-gradient, automated tuning and matching accessory, and a BTO-2000 accessory for temperature control. The routines included in the TOPSPIN 3.0 software (Bruker BioSpin GmbH, Germany) were used to perform tuning and matching, locking and shimming, and to optimize the NMR condition. Samples were measured at 343 K after a 25 min waiting period for temperature equilibration. Chitosan powder (1% v/v) was dissolved in D_2O and deuterated acetic acid (0.8% v/v) medium.

The degree of acetylation was calculated using **Equation 1.**

$$\mathrm{DS(Ac)}\ \% = (1 - (\frac{1}{3} HAc / \frac{1}{6} H_{26}))x100 \qquad (1)$$

About FTIR-ATR technique, various procedures using different absorption ratios were already proposed to determine the DS(Ac). However, the use of the amide I absorption band (*ca.*1655 cm^{-1},in our case at 1637 cm^{-1}) combined with the hydroxyl absorption band (*ca.*3450 cm^{-1}) as a reference appears to provide the best results. The **Equation 2** has been then used in these procedures and shown below. Our choice of expression used for calculation of DS(Ac) was based on literature recommendations.

$$\mathrm{DS(Ac)}\ \% = [100 - (\frac{A_{1637}}{A_{3450}})\ \mathrm{x}\ 115] \qquad (2)$$

The structures of acetylated or deacetylated monomers of Chitosan were presented in the inset of the Figure S1 reported below.In the same Figure is presented the 700 MHz ^{1}H NMR spectrum of Chitosan hydrogel at 343 K.

The assignment of Chitosan peaks was already been reported in the literature both for NMR and IR analysis. In the Table reported below are reported peaks assignment for NMR analysis.

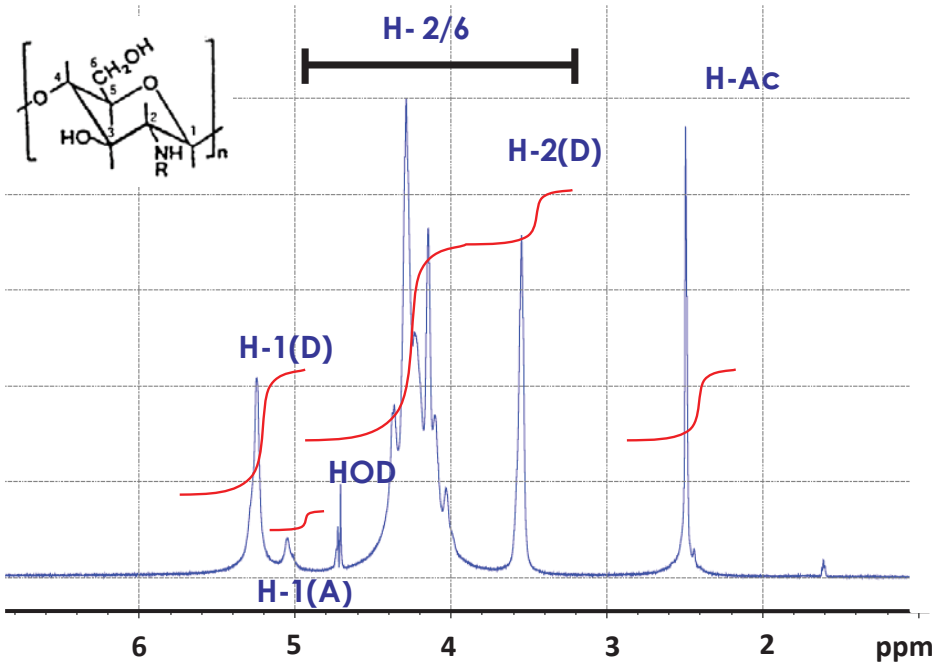

	Protons			
NMR				
	H1-A	**H1-D**	**H2-6**	**H-Ac**
Chemical shift(ppm)	5.36	5	4.20	2.50
Integral	1.18	0.31	6.6	1

Figure S1. **Top panel**: ^{1}H NMR spectra at 343 K of CH STD, realized in hydrogel condition. The structure of deacetylated or acetylated Chitosan monomer were showed. R moiety could be H for deacetylate monomer, Ac for the acetylated one. **Bottom Panel:**Chemical shifts and relative area of ^{1}H NMR signals

Procedure for Chitosan Film preparation: CH powder was dissolved in 0.1% (v/v) aqueous acetic acid solution, in order to obtain a 2% (w/v) of Chitosan, by constant continuous stirring for 24 hrs to obtain an homogeneous solution. 200μL of glycerol were added every 100 mL of CH acetic solution. Then, the solution was filtered through a coarse sintered glass filter due to the great amount of CH not dissolved and degassed for 1 hr. The reduced acetic acid amount and the excess of CH ensures the almost neutral pH at 6 units. After degassing, the CH solution was poured into a plastic Petri plate. The latter was maintained in an oven at 60˚C for 24 hrs. A thin (CH) membrane was obtained. The same procedure was followed to obtain (CH/CD) films modified with 2-HP-β-CD used as a cross-linker. In particular, the 2-HP-β-CD powder was added to chitosan hydrogel obtaining a solution having a final concentration of 10^{-3} M.

The difficulty of incorporating water insoluble Chl*a* molecules in CH/CD films has been circumvented by means of the casting technique from EtOH solution: 2×2 cm squared pieces of CH/CD free standing films were soaked with an EtOH solution containing Chl*a* (10^{-3}M) at 25 °C for 24 hrs resulting in a successful entrapment of the pigment inside the as prepared films. The outer surface of CH/CD/Chl*a*-modified films were washed with double-distilled waterand air-dried before performing any characterization. All samples have been analyzed at least in triplicate.

X-ray Photoelectron Spectroscopy (XPS) analysis.

Survey (0–1400 eV) and high resolution (C1s, O1s, N1s and Mg1s) spectra were recorded in FAT (fixed analyzer transmission) mode at pass energy of 200 and 100 eV, respectively. All spectra were acquired at a take-off angle of 37° with respect to the

sample surface. Charge compensation was accomplished by a low energy electron flood gun (1 eV). Special care was devoted during the analysis to verify that no change in the samples was induced by exposure to the X-ray beam and the electron flood gun. XPS analysis was repeated on three different spots for each sample. Charge correction of the spectra was performed by taking the hydrocarbon (C-C, C-H) component of the C1s spectrum as internal reference (binding energy, BE = 285.0 eV). Atomic percentages were calculated from the high resolution spectra using the Scofield sensitivity factors set in the ThermoAvantage V4.87 software (Thermo Fisher Corporation) and a non-linear Shirley background subtraction algorithm. The best-fitting of the high-resolution XPS spectra was performed using with mixed Gaussian-Lorentzian peaks after a Shirley background subtraction; a maximum relative standard deviation of 10% was estimated on the area percentages of the curve-fitting components, while the determined standard deviation in their position was ± 0.2 eV.

Differential Scanning Calorimetry (DSC).

For thermogram acquisition, sample sizes of 1 to 2 mg were scanned with a heating rate of 5°C/min over a temperature range from 25°C to 300°C. Dry material was placed in an aluminum cup and hermetically sealed. Chl*a* samples were prepared by casting from ethanol solution in the aluminum caps. Empty cup was used as a reference and runs were performed in triplicate. Samples were analyzed under continuous flux of dry nitrogen gas (50 mL/min).

Water Vapor Transmission Rate (WVTR).

The instrument displays the WVTR as either $g/m^2/day$ or g/100in2/day and into the instrument is incorporated a Pb_2O_5 sensor. According to the Faraday's Combined Laws

of Electrolysis, the electrolytic current is a measure of the rate at which water is electrolyzed. Under equilibrium conditions this equals the rate at which moisture is being absorbed by the Pb_2O_5 film. Thus, knowledge of the gas flow rate through the housing and the current in the cell gives an absolute measure of the moisture contained in the sample gas. The films were stored in the cell at 25 ± 1 °C and 90 ± 1% relative humidity (RH) for 24 hrs.

Information related to Laser flash photolysis setup

The sample was excited with the third harmonic of a Nd–YAG Continuum Surelite II–10 laser (355 nm, 6 ns, ~ 10 mJ). The quartz plate with the chitosan-based film was aligned at an angle of 45° with respect to both the excitation and the monitoring beams. The reflection of the excitation from the quartz plate was to the opposite side of the transient signal detection. The measurements in solution were carried out with a 10 × 10 mm^2 quartz cell with a 3 mL capacity. The excited samples was analyzed with a Luzchem Research mLFP–111 apparatus with an orthogonal pump/probe configuration. The probe source was a ceramic xenon lamp coupled to quartz fiber-optical cables. The laser pulse and the mLFP–111 system were synchronized by a Tektronix TDS 3032 digitizer, operating in pre-trigger mode. The signals from a compact Hamamatsu photomultiplier were initially captured by the digitizer and then transferred to a personal computer, controlled by Luzchem Research software operating in the National Instruments LabView 5.1 environment. The sample temperature was 295 ± 2 K. The energy of the laser pulse was measured at each shot with a SPHD25 Scientechpyroelectric meter.

Direct detection of $^1O_2$.

Steady-state emission of $^1O_2$ in the NIR region was recorded with a Fluorolog-2 Mod-111 spectrometer, equipped with a InGaAs detector maintained at –196 °C, by illuminating the film sample, immersed in a quartz cuvette filled D_2O and placed at 45° with respect the excitation beam, with a 405 nm CW laser (2 W cm^{-2}).

Photoactivity measurements.

In order to demonstrate the photoactivity of chitosan film containing Chl*a*, direct and indirect methods were employed to achieve our aim. 4-thiothymidine (S^4TdR, Carbosynth Limited, UK) and Singlet Oxygen Sensor Green (SOSG, Molecular Probes, Inc. by Life Technologies Limited, Scotland) have been used in aqueous solution at concentration of 10^{-5} M and 1.5 μM, respectively. These aqueous solutions containing a slice film 1×1 cm were illuminated with a neon lamp, whose emission had been previously assessed to occur mainly between 400 and 700 nm and with a power surface density of 60mW/cm^2. The solution absorption or emission spectra were recorded at different times of irradiation. S^4TdR absorption spectra were recorded in the range of 200-800 nm (λ^{max} = 337 nm in aqueous solution and 326 in D_2O). SOSG emission was registered at 525 nm (λ_{ex} = 488 nm). Its maximum absorption peak was at about 500 nm. Chitosan film containing-Chl*a* absorption spectra were recorded in the range of 350-800 nm.

As far as SOSG, it is reported in literature as a highly selective singlet oxygen fluorescent probe with a fluorescein moiety bound to an anthracene derivative. The reaction with singlet oxygen increases the observed emission at 525 nm due to the generation ofan endoperoxide specie as a main product. A 550 nm cut-off glass filter has been used to reduce the self-production of $^1O_2$ by SOSG. Measurements were achieved before irradiation and every 10 minutes for 100 minutes. As far as S^4TdR is

concerned, it is a modified nucleoside able to react with singlet oxygen without, at moment, selectivity in the presence of ROS. Moreover our recent studies show its high photostability, if solution was irradiated with visible light. Measurements were achieved before irradiation and after 100 minutes.

As far as the irradiation of Chitosan film-containing Chl*a*, it has been realized, directly, with a slice film (1×1 cm) putted on neon lamp, and UV-Visible absorption-measurements have been performed before irradiation and every 10 minutes for 100 minutes employing a supporting film-device. The fluorescence measurements were conducted using a spectrofluorimeter Varian CARY Eclipse 68. A quartz cuvette with an optical path length of 1 cm has been employedfor all spectroscopic measurements.

Extraction of Chl*a*

The extraction of Chl*a* from spinach leaves has been carried out using the procedure of Omata and Murata. It involves 3 main steps:

1. Activation of resins used as stationary phase for chromatographic separation;

2. Photosynthetic pigments extraction (Chl*a* and *b*);

3. Pigment separation.

Procedure of resin activation

For the two subsequent chromatographic separations, ion exchange resins were used and they need to be preliminary activated. The first resin used is the DEAE-Sepharose CL-6B (Sigma-Aldrich), whose DEAE acronym indicates the functionalization with diethylaminoethylenic groups [-$OCH_2CH_2N(CH_2CH_3)_2$]. It was washed with a great amount of distilled water, stirring with a glass rod. Then, it is left in suspension with a solution of sodium acetate (CH_3COONa) 1 M at pH 7. Subsequently, the resin was washed with distilled water and then

with a great volume of acetone. The activated resin was stored as a suspension in acetone at +4°C.

The second resin is Sepharose CL-6B (Sigma-Aldrich). It was initially washed with a great amount of distilled water, stirring with a glass rod. The subsequent washing operations were performed using (i) acetone, (ii) acetone-hexane (2:1), (iii) acetone-hexane (1:2), (iv) hexane-isopropanol (10:1) and (v) hexane-isopropanol (20:1). The activated resin is kept in the last solvent mixture at a temperature of +4°C.

Procedure of photosynthetic pigment extraction

Approximately 30 g of fresh spinach leaves were carefully washed to remove residual of soil and sand. Then, they were homogenized in 200 mL of acetone in the presence of 500 mg of $Na_2HPO_4 \cdot 12H_2O$, whose function was to ensure a neutral pH in order to prevent the chlorophyll pheophytinization, *i.e.* the loss of the central magnesium ion. The mixture was filtered under vacuum on a Buchner funnel. The filtrate was treated with dioxane and a minimal amount of distilled water necessary for the occurrence of a green precipitate, the complex chlorophyll-dioxane. The solution was then stored at -20°C in order to furtherly facilitate the precipitation.

Procedure of pigment separation

The first column was packed with activated DEAE-Sepharose CL-6B and the separation was carried out at 4 °C. Acetone was used as first elution solvent. The quickly formation of two bands were observed. The former, appearing green in color, containing chlorophylls, remained at the head of the column, the latter, yellow, containing carotenoids and pheophytins, was eluted quickly.

Changing eluent and using a mixture of acetone-methanol 10:3, chlorophylls *a* and *b*, together with small amounts of glycolipids were eluted from the column and collected in a flask and introduced in the second column packed with Sepharose CL-6B resin. A mixture of hexane-

isopropanol 20:1 was the first elution solvent used; in this condition the separation of Chl *b* from Chl *a* was obtained.

SUPPORTING RESULTS

Water Vapor Transmission Rate

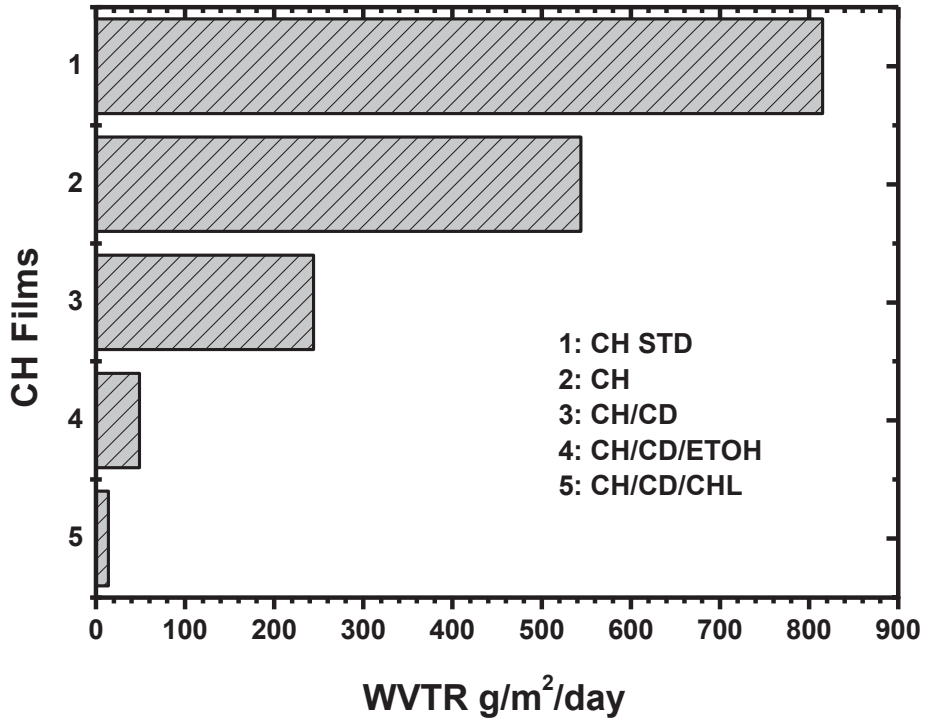

Figure S2: Comparison between WVTR obtained for all studied CH films.

X-ray Photoelectron Spectroscopy

Table S2. XPS surface atomic concentrations of **(a)** the CH film prepared with the new methodafter immersion in ethanol,**(b)** the CH/CD film after immersion in ethanol and **(c)** the CH/CD/Chl*a* film.

Signal	Atomic concentration [%][a)]		
	(a) CH + EtOH	(b) CH/CD + EtOH	(c) CH/CD/Chl a [a)]
C 1s	63 ± 2	62.2 ± 1.5	73.0 ± 1.0
N 1s	6.0 ± 0.5	4.8 ± 0.3	2.6 ± 0.20
O 1s	31 ± 2	33.0 ± 1.0	19.0 ± 0.6
Mg 1s	--	--	0.38 ± 0.13

[a)] XPS analyses revealed the presence of silicon in the CH/CD/Chl*a* film (atomic percentage of about 5%) associated to a silica/glass fiber contamination not totally removed during the Chl*a* work up procedure.

Scanning Electron Microscopy

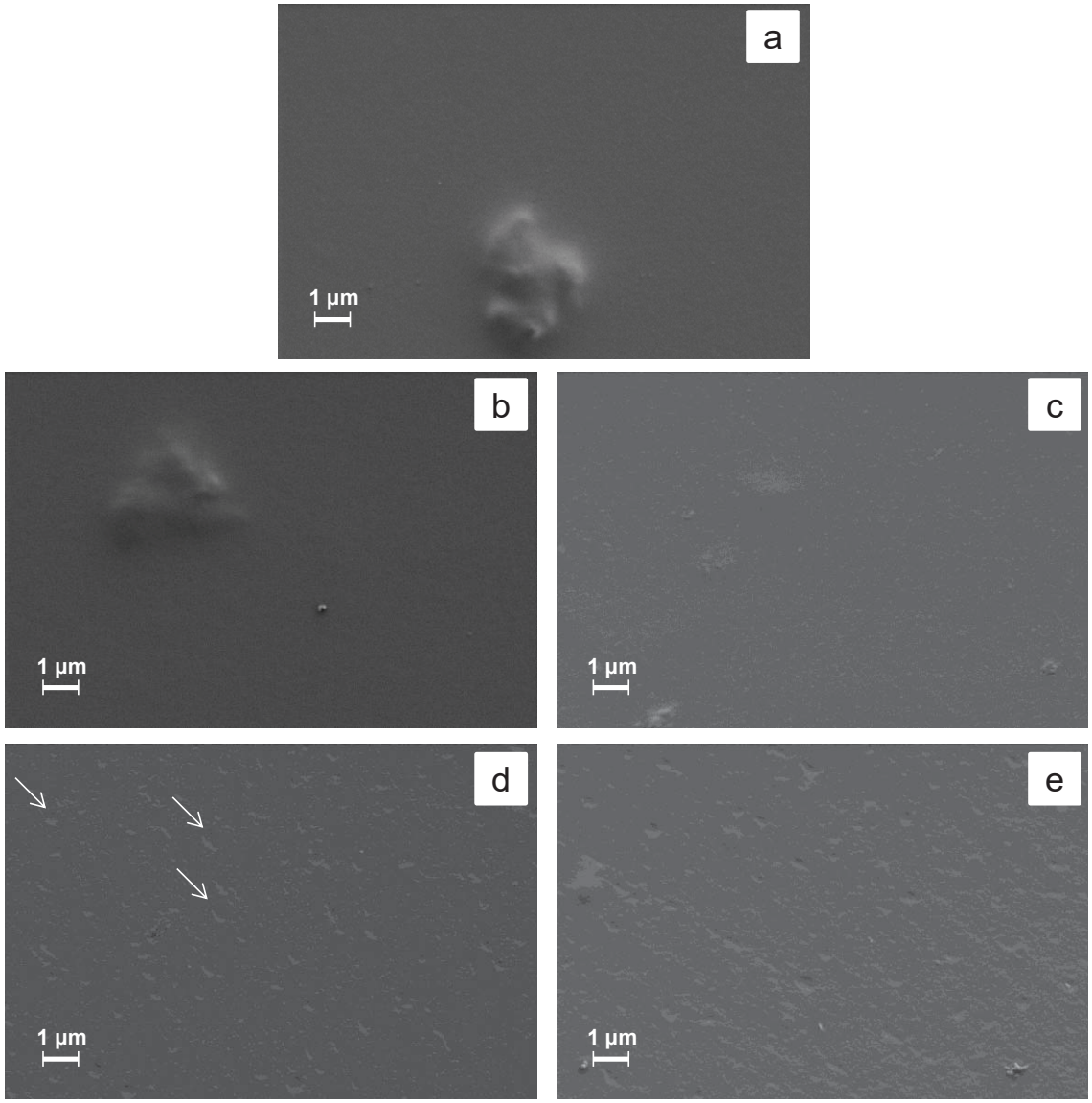

Figure S3: SEM images of **(a)** CH film prepared with the standard method, **(b)** CH film prepared with the new method (the result occurs the same in the presence of CD); **(c)** CH film prepared with the new method after immersion in ethanol, **(d)** CH/CD film after immersion in ethanol, **(e)** CH/CD/Chl*a* film

Atomic Force Microscopy

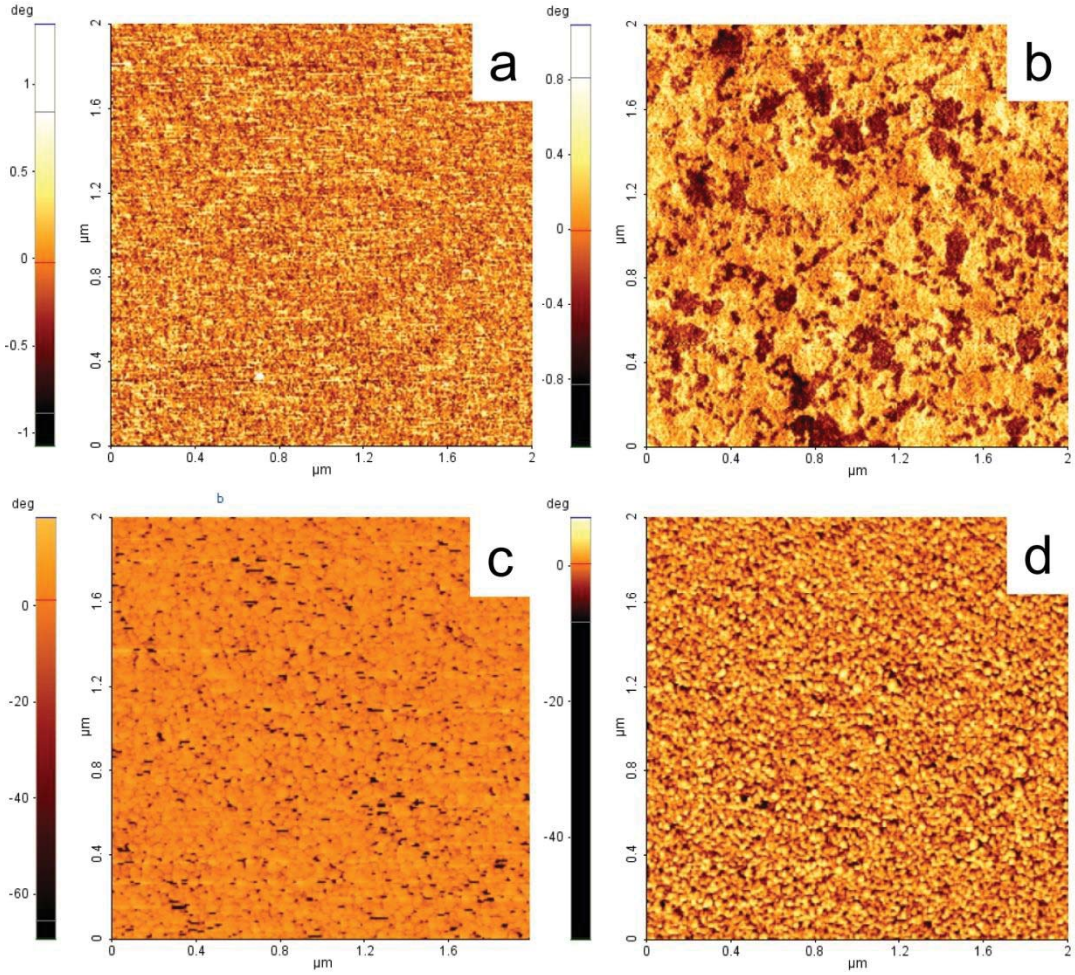

FigureS4: Corresponding AFM Phase images of "as prepared" **(a, b)** and upon treatment with EtOH **(c, d)** related to CH and CH/CD films, respectively.

X-ray diffraction

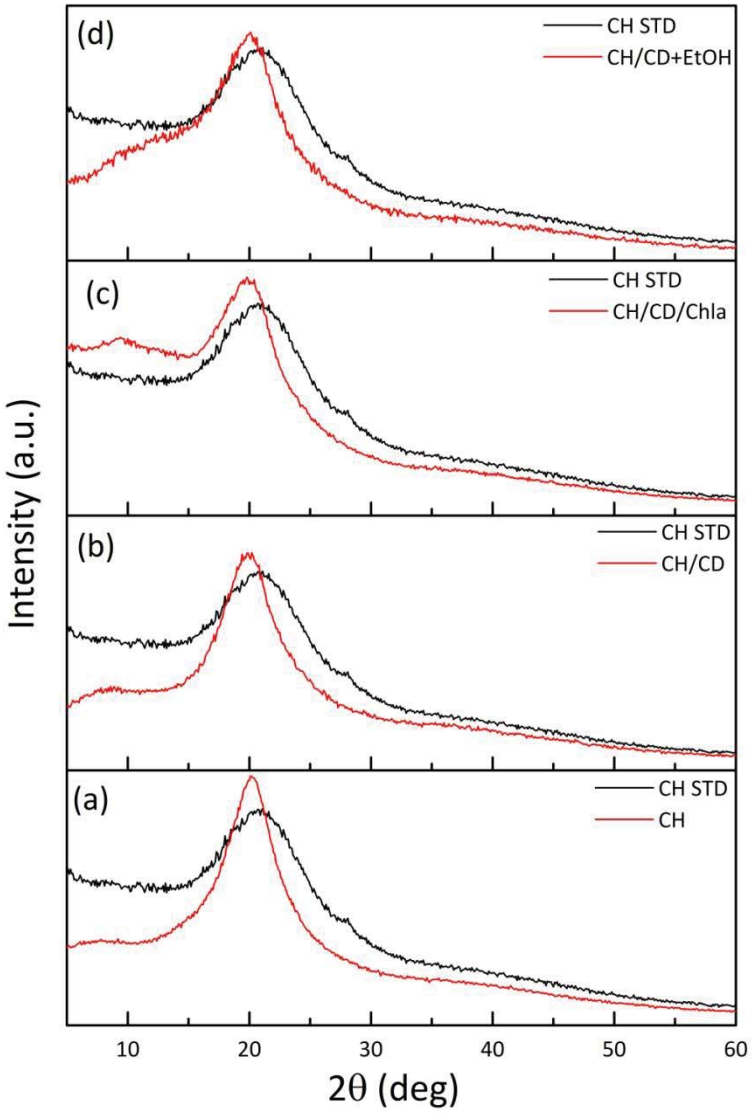

Figure S5:Comparison between XRD pattern of the chitosan film prepared according the standard procedure (CH STD) and **(a)** the modified one (CH), **(b)** the chitosan film containing 2-HP-β-CD (CH/CD), **(c)** the chitosan film containing 2-HP-β-CD and Chl*a* (CH/CD/Chl*a*), **(d)** the chitosan films containing 2-HP-β-CD after treatment with EtOH (CH/CD + EtOH).